nature communications

Article

https://doi.org/10.1038/s41467-025-57165-2

Pluripotency factor Tex10 finetunes Wnt signaling for spermatogenesis and primordial germ cell development

Received: 22 March 2022

Accepted: 13 February 2025

Published online: 23 February 2025

Check for updates

Feifei Yuan[1,4], Jihong Yang[1,3,4], Fanglin Ma[2,4], Zhe Hu[1], Vikas Malik[1], Ruge Zang[1], Dan Li[1], Xianle Shi[1], Xin Huang[1], Hongwei Zhou[1] & Jianlong Wang[1]

Testis-specific transcript 10 (Tex10) is highly expressed in the testis, embryonic stem cells (ESCs), and primordial germ cells (PGCs). We previously generated a Tex10 knockout mouse model demonstrating its critical roles in ESC pluripotency and preimplantation development. Here, using conditional knockout mice and dTAG-degron ESCs, we show Tex10 is required for spermatogenesis and ESC-to-PGCLC differentiation. Specifically, Tex10-null spermatocytes arrest at metaphase I, compromising round spermatid formation. Tex10 depletion and overexpression compromise and enhance ESC-to-PGCLC differentiation, respectively. Mechanistically, bulk and single-cell RNA sequencing reveals that Tex10 depletion downregulates genes involved in pluripotency, PGC development, and spermatogenesis while upregulating genes promoting somatic programs. Chromatin occupancy study reveals that Tex10 binds to H3K4me3-marked promoters of *Psmd3* and *Psmd7*, negative regulators of Wnt signaling, and activates their expression, thereby restraining Wnt signaling. Our study identifies Tex10 as a previously unappreciated factor in spermatogenesis and PGC development, offering potential therapeutic insights for treating male infertility.

Infertility is a global concern affecting approximately 10–20% of couples worldwide, and 30–50% of cases are caused by male factors[1]. Male infertility is increasingly recognized as both a disease and a significant public health issue, significantly impacting the quality of life for affected individuals and their partners[2]. Spermatogenesis is a highly intricate and precisely regulated process from which sperms are produced from primordial germ cells (PGCs). Germ cells integrate into the sex cords, maturing into seminiferous tubules lined with Sertoli cells that support and anchor the germ cells, enabling their development into mature sperms[3]. Impairments in spermatogenesis are the most common underlying cause of male infertility[4]. Remarkably, there are currently no FDA-approved medications available for treating male infertility[5]. Thus, it is urgently necessary to study critical molecular players in the male germline that can serve as future therapeutic targets.

PGC specification in humans and mice is followed by migration, colonization, sex determination, and PGC differentiation to either sperms or oocytes[6]. An increasing effort has been made to search for critical factors in the PGC specification[7,8]. In mice, PGC specification follows the BMP- and Wnt-dependent induction, which promotes the activation of several important PGC specifiers[9] such as Prdm1, Prdm14, and AP2γ. These factors further form a self-reinforcing network promoting germ cell development and pluripotency gene reactivation while feeding back to repress other Wnt-induced mesoderm genes[9,10].

[1]Department of Medicine, Columbia Center for Human Development and Stem Cell Therapies, Columbia Stem Cell Initiative, Herbert Irving Comprehensive Cancer Center, Columbia University Irving Medical Center, New York, NY, USA. [2]Department of Cell, Developmental and Regenerative Biology; The Black Family Stem Cell Institute, Icahn School of Medicine at Mount Sinai, New York, NY, USA. [3]Present address: BoYu Intelligent Health Innovation Laboratory, Hangzhou, China. [4]These authors contributed equally: Feifei Yuan, Jihong Yang, Fanglin Ma. e-mail: jw3925@cumc.columbia.edu

Notably, both aberrant Wnt activation and inhibition impair PGC specification in vitro, i.e., induction of PGC-like cells (PGCLCs) from pluripotent ESCs[8], suggesting that precise Wnt activity levels are necessary for optimal PGC specification. The role of Wnt signaling in spermatogenesis is complex: while Wnt/β-catenin signaling promotes spermatogonia stem/progenitor cell proliferation[11,12], overactivation can cause germ cell defects and premature loss[13,14]. A notable feature of PGC specification is the reactivation of pluripotency. Accordingly, many pluripotency factors play important roles in PGC specification, exemplified by the positive roles of the core pluripotency factors Nanog[7], Oct4[15], and Sox2[16], whose loss compromises PGC specification and causes cell death. In contrast, primed pluripotency factor Otx2[17,18] restricts PGC specification[19].

Among the TEX family genes, Tex10 is a pluripotency regulator that functions as a partner of Nanog, Oct4, and Sox2, as we reported previously[20]. Tex10 knockdown in embryonic stem cells (ESCs) using small-hairpin RNAs (shRNAs) causes cell differentiation/apoptosis and, consequently, the loss of pluripotency. Tex10 global knockout embryos homozygous for a gene-trapped allele are lethal at the morula to the blastocyst stage[20]. Interestingly, TEX family gene variants have been linked to human azoospermia with strong evidence, according to ClinGen[21]. In addition, 15 of 28 infertile men who were reported to carry rare potential disease-causing variants in nine TEX genes have mutations in TEX10, TEX27, and TEX33[22], highlighting TEX10 as the new variant associated with male infertility. Surprisingly, though, the knockdown of Tex10 in Drosophila resulted in normal fertility[22]. Therefore, more research is needed to confirm TEX10's functional role in male germ cell development in mammals.

In this study, we created a *Tex10* conditional knockout (cKO) mouse model combined with a male germline-specific (Stra8) Cre mouse. We performed bulk and single-cell RNA sequencing (scRNA-seq) to further explore the role of Tex10 in spermatogenesis. We found that male mice deficient in *Tex10* exhibited reduced sperm count and motility and impaired round spermatid formation caused by an arrest in metaphase I spermatocyte during spermatogenesis. We further employed an ESC-to-PGCLC differentiation model with engineered Tex10 inducible depletion (i.e., dTAG-degron) and constitutive overexpression mouse ESC lines for transcriptome and genome-wide chromatin occupancy studies. We uncovered a critical role of Tex10 in restraining Wnt signaling, partly through direct transcriptional activation of Psmd3 and Psmd7, two negative regulators of Wnt signaling, during ESC-to-PGCLC differentiation and likely also during spermatogenesis. Thus, our study establishes the pluripotency factor Tex10 as a previously unappreciated molecular player essential for spermatogenesis and germ cell development.

Results

Tex10 is highly enriched in male germ cells

As expected for its function in ESCs[20] and its name/origin as the "testis-specific transcript-10", Tex10 is highly enriched in ESCs and testis based on Biogps.org (Fig. S1a), suggesting its potential roles in spermatogenesis beyond its established roles in pluripotency control[20]. Reanalyzing the single-cell RNA-seq (scRNA-seq) data from 28 critical time-points across the male mouse germ cell development process[23], we found Tex10 was abundantly expressed in spermatogenic cells, encompassing spermatogonia (Spg), spermatocytes at leptotene, zygotene, pachytene, diplotene, and metaphase I stages (L/Z/P/D/MI Sct), and round spermatids (RS) (Fig. 1a). We performed immunostaining with undifferentiated spermatogonia (undiff.ed Spg) marker PLZF and germ cell marker DDX4, confirming that Tex10 protein was highly expressed in the Spg, especially in undiff.ed Spg, Sct, and RS (Fig. 1b, c). In contrast, Tex10 is barely expressed in Sertoli cells (SC) and Leydig cells (LC) based on a LacZ gene-trapped Tex10 allele[20] (Fig. S1b, c). These protein expression data are consistent with the Tex10 RNA expression profile; however, Tex10 transcripts are readily detectable in somatic cells of mesoderm and mesenchyme lineages (Fig. 1a). Surprisingly, Tex10 is also expressed in the primary and growing oocytes in the female germ line (Fig. S1d, e and Supplementary Data 1, data from GSE75738[24]).

PGC development is associated with the reactivation of the pluripotency program encompassing the expression of the core pluripotency factors Nanog, Oct4, and Sox2. Consistent with it being the partner protein[20] of Nanog, Oct4, and Sox2, Tex10 was highly expressed in PGCs across embryonic developmental stages (from specification to post-mitotic arrest) (Fig. 1a), based on the reanalysis of scRNA-seq data from male mouse germ cell development[23]. By performing in vitro ESC-to-PGCLC induction[25] followed by immunostaining of whole embryonic bodies (EBs) with Tex10 and germ cell marker AP2γ (Fig. S1f and Methods), we confirmed Tex10 protein expression in PGCLCs and non-PGCLCs similarly at days 2 and 4 but with a significantly higher level in PGCLCs than non-PGCLCs at day 6 (Fig. 1d, e). We further conducted a gene prioritization analysis in 30 tissues/cells (see Method sections for detail), focusing on early embryos (such as 4-cell, 8-cell, morula, and blastocyst), ESCs, epiblast, and PGCs (male/female). We identified 9 and 8 genes with the highest expression levels (ranks#1) in the male and female PGCs, respectively (Fig. S1g). Like *Prdm1*, which shows high expression levels in both male (rank#1) and female (rank#2) PGCs (Fig. S1h), *Tex10* also shows high expression levels in both male (rank#1) and female (rank#5) PGCs (Fig. 1f). Together, these data indicate that Tex10 is highly enriched in germ cells, particularly of male germline, suggesting it could be a novel regulator for spermatogenesis and PGC development.

Tex10 is functionally important for male fertility

Tex10 conventional knockout embryos die at the preimplantation stage[20], precluding the analysis of Tex10's functional contribution to germ cell development. To obviate this hurdle, we employed CRISPR genome editing to create the *Tex10*$^{fl/fl}$ mice (Fig. S2a, b; see Methods for detail). Then, *Tex10*$^{fl/fl}$ mice were crossed with *Stra8*-iCre[26] transgenic mice to generate *Tex10* conditional knockout (*Tex10*-cKO) mice with the genotype of *Tex10*$^{fl/-}$*;Stra8*-iCre, from which *Tex10* was knocked out starting from differentiated spermatogonia and persisting throughout the later stages of the male germline. For simplicity, we defined all mice with *Tex10*$^{+/+}$, *Tex10*$^{fl/fl}$, and *Tex10*$^{f/+}$ genotypes as control mice and those with *Tex10*$^{fl/-}$*;Stra8*-iCre genotype as cKO mice. We confirmed a significant reduction of Tex10 expression by qPCR, western blot, and immunostaining in adult (8-week-old) *Tex10* cKO testes relative to control testes (Fig. S2c–e). *Tex10* cKO mice were subfertile and displayed smaller testes than control mice (Fig. 2a–c). Histological analysis revealed that the number of spermatids decreased significantly in the *Tex10* cKO seminiferous tubules and that there are abnormal round spermatids (marked with black arrows) detached from the seminiferous epithelium in *Tex10* cKO but not the control testis (Fig. 2d). Also, the vacuoles of seminiferous tubules (marked with red asterisks), often observed in defective spermatogenesis[27], increased significantly in *Tex10* cKO testis (Fig. 2d, e). Accordingly, sperm counts from epididymis cauda dramatically declined in *Tex10* cKO epididymis cauda (Fig. 2d, f). Importantly, *Tex10* cKO sperms displayed abnormal shape (marked with red arrows, Fig. 2g) with reduced mobility compared to the control mice (Supplementary Movie 1 for control and Supplementary Movie 2 for *Tex10* cKO). Consistently, roughly only half (51.45 ± 13.69%) of seminiferous tubules contain PNA lectin (a marker of spermatids) in *Tex10* cKO testis (Fig. 2h, i).

Next, we extracted the RNA from the whole testes of adult control and *Tex10* cKO mice for RNA sequencing (RNA-seq). Gene Set Enrichment Analysis (GSEA) of differentially expressed genes on the hallmark dataset confirmed that spermatogenesis was significantly compromised in *Tex10* cKO mice (Fig. 2j and Supplementary Data 2). In particular, spermatogenesis genes, such as *Akap4*[28], *Papolb*[29,30],

https://doi.org/10.1038/s41467-025-57165-2

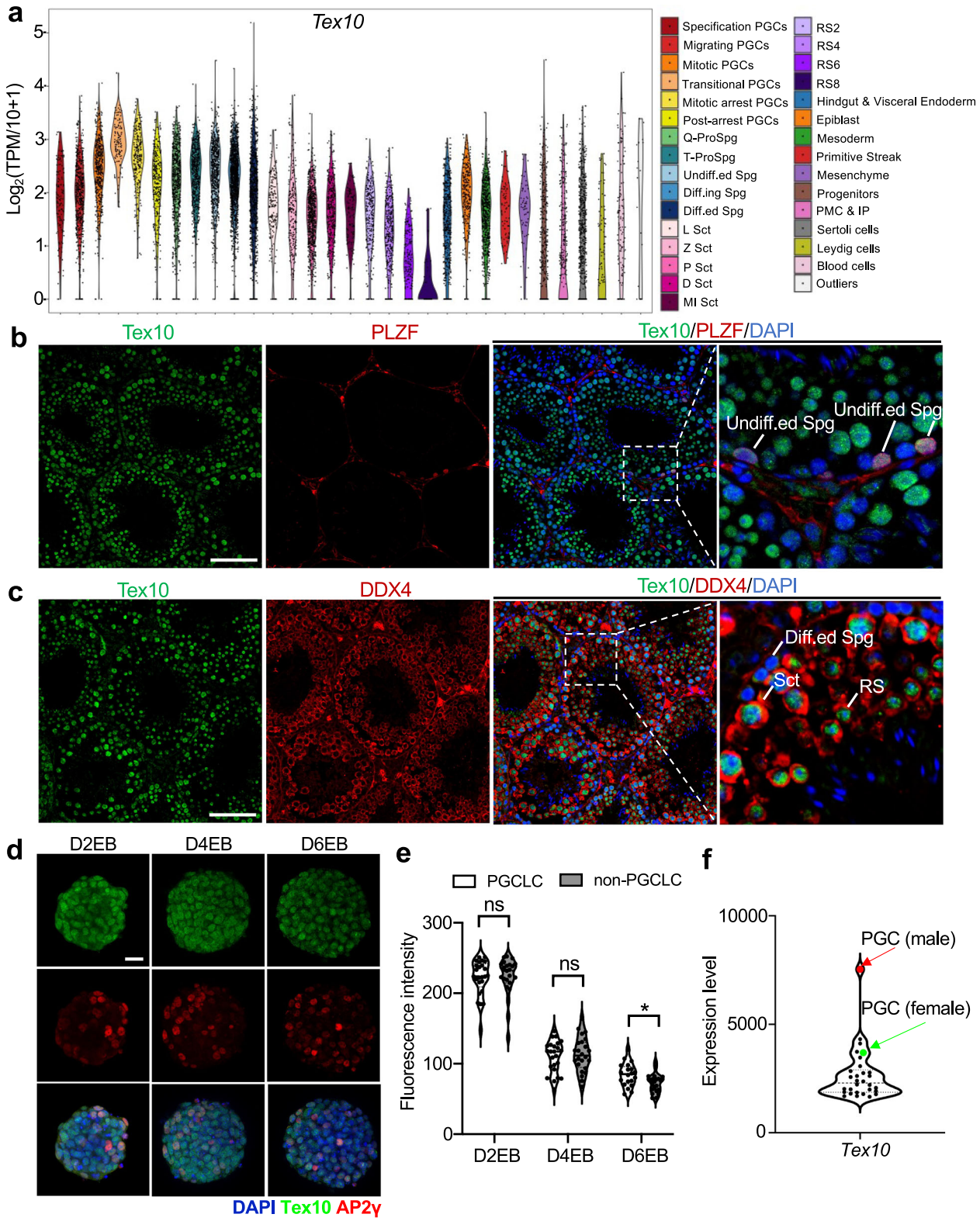

Fig. 1 | Tex10 is highly enriched in male germ cells. a Single-cell RNA-seq reanalysis of *Tex10* expression level in PGC, spermatogenic cells from adult mice, and somatic cells. Data was obtained from GSE148032[23]. **b** Immunostaining of Tex10 and PLZF in testis sections from adult (8-week-old) mice. The right panels show enlarged images of indicated areas. Undiff.ed Spg, undifferentiated spermatogonia. DAPI shows the nucleus. Scale bar, 100 μm. **c** Immunostaining of Tex10 and DDX4 in testis sections from adult mice. The right panels show enlarged images of indicated areas. Diff.ed Spg, differentiated spermatogonia. Sct, spermatocyte, RS, round spermatid. DAPI shows the nucleus. Scale bar, 100 μm. **d**, **e** Immunostaining (**d**) and quantification (**e**) of Tex10 and AP2γ in PGCLCs (Tex10+ and AP2γ+) and non-PGCLCs (Tex10+ and AP2γ−) from day 2, day 4 and day 6EBs. DAPI shows the nucleus. Scale bar, 20 μm. Quantification (**e**) was performed with a two-sided student's *t* test. Error bars, mean ± SD. $p = 0.0149$ (*) and $p > 0.05$ (ns). Source data are provided as a Source Data file. **f** A violin plot showing mouse tissue/cell (sample number: $n = 30$) expression of Tex10. The male PGC sample is shown in red, and the female PGC in green; black dots represent the remaining 28 tissue/cell samples.

https://doi.org/10.1038/s41467-025-57165-2

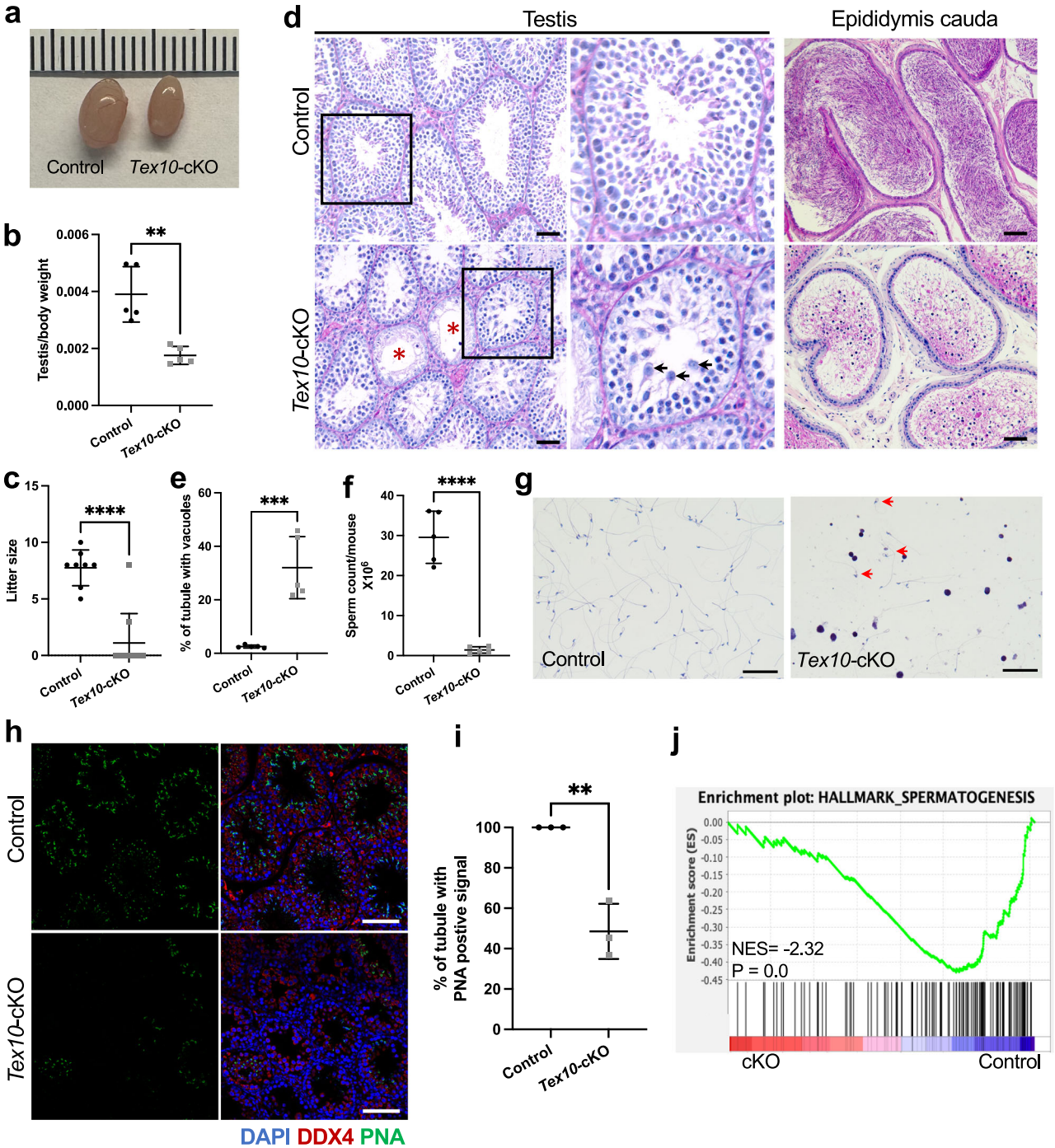

Fig. 2 | Conditional knockout of Tex10 reveals its role in spermatogenesis and male infertility. a Morphology of representative testes from adult control and *Tex10*-cKO mice. **b** The testis and body weight ratio of control and *Tex10*-cKO adult mice ($n = 5$ mice per condition). Two-sided student's *t*-test. Error bars, mean ± SD. $p = 0.0016$ (**). Source data are provided as a Source Data file. **c** The comparison of the litter sizes produced by wildtype (WT) female mice mated with control and *Tex10*-cKO mice ($n = 4$ male mice of control and $n = 5$ male mice of *Tex10*-cKO). Two-sided student's *t*-test. Error bars, mean ± SD. $p < 0.0001$ (****). Source data are provided as a Source Data file. **d** PAS staining in testis and epididymis sections of control and *Tex10*-cKO adult mice. The red asterisks indicate vacuoles exhibited in seminiferous tubules. Arrows indicate detached round spermatids. Scale bar, 100 μm. **e** The percentage of seminiferous tubules containing vacuoles from control and *Tex10*-cKO adult testis sections ($n = 5$ mice per condition). Two-sided student's *t*-test. Error bars, mean ± SD. $p = 0.0005$ (***). Source data are provided as a Source Data file. **f** The quantification of sperm count from epididymis cauda of control and *Tex10*-cKO adult mice ($n = 5$ mice per condition). Two-sided student's *t*-test. Error bars, mean ± SD. $p < 0.0001$ (****). Source data are provided as a Source Data file. **g** Morphology of representative sperms derived from epididymis cauda of control and *Tex10*-cKO adult mice. The red arrows indicate abnormal sperm shape. Scale bar, 100 μm. **h** Immunostaining of PNA (green) and DDX4 (red) in control and *Tex10*-cKO adult testis sections. DAPI shows the nucleus. Scale bar, 100 μm. **i** The percentage of seminiferous tubules containing PNA-positive cells from control and *Tex10*-cKO adult testis sections ($n = 3$ mice per condition). Two-sided student's *t*-test. Error bars, mean ± SD. $p = 0.0029$ (**). Source data are provided as a Source Data file. **j** GSEA plots of spermatogenesis obtained using bulk RNA-seq data on control and *Tex10*-cKO adult testes.

Ccna1[31–33], and *Tulp2*[34], sperm motility-related genes, such as *Oaz3*[35], *Spata6*[36], and *Odf1*[37–40], and round spermatid-related genes, such as *Tnp1*[41], *Tnp2*[41], and *Tbpl1*[42], were all downregulated (Fig. S2f, g). Of note, Tex10-deficient oocytes, generated by the female germline-specific *Zp3*-Cre that acts in the growing oocyte[43], are morphologically and functionally normal (Fig. S2h, i), highlighting male germline-specific functions of Tex10.

Interestingly, a significant *TEX10* downregulation was observed in patients with severely impaired spermatogenesis (Fig. S2j and Supplementary Data 3, data from GSE145467[44]) and infertile teratozoospermia individuals compared with fertile normospermia individuals (Fig. S2k and Supplementary Data 4, data from GSE6872[45]). Such testis[44]- and sperm[45]-specific reduction of *TEX10* RNA expression in infertile relative to normal fertile men suggests the potential involvement of TEX10 in human spermatogenesis and/or spermiogenesis. However, it is unclear whether a specific germ cell type downregulates TEX10 expression or whether the proportion of those germ cells expressing TEX10 is reduced within the testis samples of the patients under study[44]. Nonetheless, recent studies applying single-cell analysis of developing and azoospermia human testicles[46,47] provided another convincing example of a pronounced reduction of *TEX10* expression in spermatogonia and spermatids of AZFa_Del and NOA infertile men (Fig. S2l). Together, these results support an evolutionarily conserved and critical role of Tex10 in male germline development.

Tex10 deficiency causes spermatocyte arrest at meiotic metaphase I and compromises round spermatid formation

To pinpoint the stage when spermatogenesis is compromised by Tex10 depletion, we first employed the FACS approach[48] to distinguish cells from testes of adult control and *Tex10* cKO mice, identifying Spg, Sct at meiosis I (MI) and meiosis II (MII), and RS populations (Fig. S3a). Importantly, we found that Tex10 depletion significantly increased the Sct and decreased the RS population. In contrast, the Spg population was not significantly affected (Fig. 3a). Then, we performed TUNEL staining and found increased apoptotic cells in *Tex10* cKO seminiferous tubules (Fig. 3b, c), suggesting the clearance of germ cells without Tex10 through programmed cell death. We further examined DNA double-strand breaks (DSBs) and homologous chromosome synapsis by immunostaining γH2AX and SYCP3, respectively, on chromosome spreads of meiotic prophase spermatocytes (Fig. 3d, e) and seminiferous tubules (Fig. S3b). We found that γH2AX signals (green) in Tex10-null spermatocytes were distributed around all chromosomes (red SYCP3 signals) at the leptotene and zygotene stages, then disappeared from autosomes but remained in XY body at the pachytene and diplotene stages (Fig. 3d). The proportion of each type of spermatocytes was similar to controls (Fig. 3e), indicating that Tex10-null spermatocytes are not arrested at prophase I. Next, we performed immunostaining against the metaphase cell marker phospho-histone H3 (Thr3) (pH3) and γH2AX in the seminiferous tubules to characterize meiotic metaphase I. We found that the number of tubules containing pH3+ spermatocytes was significantly increased in adult *Tex10*-cKO testis (Fig. 3f, g), consistent with the histology analysis (Fig. 3h). These findings demonstrate that Tex10 deficiency leads to Sct arrest at MI with compromised RS formation.

Tex10 regulates the Sct-to-RS transition through transcriptional control of meiosis and spermatic maturation genes

To gain insight into the molecular mechanism by which Tex10 regulates spermatogenesis, we conducted bulk RNA-seq of FACS-purified spermatogenic cells and scRNA-seq of whole cell populations from control and *Tex10* cKO testes. Bulk RNA-seq identified 410 transcripts in spermatogonia, 388 and 273 transcripts in MI and MII spermatocytes, and 129 transcripts in spermatids significantly altered (i.e., upregulated and downregulated) in *Tex10* cKO testis compared with control (Fig. 4a and Supplementary Data 5). Genes related to spermatogonia differentiation (e.g., *Stra8, Kit*), chromosome segregation during meiosis in spermatocytes (e.g., *Aurka, Aurkb, Sycp3, Cenpl, Cenpe, Meiob*), and spermatid maturation (e.g., *Id4, Prm1, Prm2, Tnp1, Tnp2*) were dysregulated by *Tex10* deficiency (Fig. 4a, c). GSEA of RNA-seq data using cell-type-specific gene sets revealed a significant depletion of genes associated with "chromosome separation," "kinetochore organization," "microtubule-based movement," and "sperm axoneme assembly" in cKO testis (Fig. 4b), indicating the developmental defects in spermatogenic cells. Downregulation of genes associated with "kinetochore organization" and "microtubule-based movement" in *Tex10*-null spermatocytes and "axoneme assembly" in *Tex10*-null spermatids (Fig. 4b, c) suggests impaired chromosome segregation during the meiotic metaphase[49] and sperm flagellum formation[50]. These results explain the observed spermatocyte metaphase I arrest with compromised spermatid formation resulting from *Tex10* deficiency in the testis (Figs. 3 and S3).

Analyzing scRNA-seq data yielded well-defined different cell populations clustered by specific markers (Fig. S4a, b). In line with our findings in Fig. 3a, we confirmed that the Sct population was increased, whereas the RS population was decreased in *Tex10* cKO relative to control (Fig. S4c). Using pseudo-time analysis, we delineated the trajectories of cells in both the control and cKO groups. Both sets of cells initially followed a similar developmental trajectory from Spg#2 to Sct#4; at this point, they diverged into two distinct branches: one branch culminated in RS#2, while the other proceeded towards Sct#3 (Fig. 4d). However, a notable distinction emerged: unlike control cells, which continued their developmental journey from Sct#3 to RS#4 and further preSza#1 (Fig. 4d left panels), the cKO cells ceased their progression at Sct#3 (a subpopulation of cells at the Sct stage, Fig. 4d right panels). This observation suggests that *Tex10* cKO may impair the ability of Sct cells to transition into RS cells. To explore this, we performed a Gene Ontology (GO) functional enrichment analysis on the differentially expressed genes between the two Sct populations of cKO and control samples. The analysis revealed significant enrichment in meiosis I-related pathways (Fig. 4e). Additionally, GSEA showed significant downregulation of "germ cell development," "meiotic cell cycle," and "spermatid differentiation" in the cKO compared to the control sample (Fig. S4d). These results further support that Tex10 deficiency disrupts germ cell development during the Sct-to-RS transition, likely through transcriptional control of meiosis and spermatic maturation genes.

Tex10 depletion compromises the efficiency of PGC development

Given Tex10's enrichment in PGCs and PGCLCs (Figs. 1 and S1), we next explored the potential roles of Tex10 in PGC development. First, we mated *Tex10*$^{fl/fl}$ mice with *Prdm1*-Cre mice expressing Cre recombinase under the control of the early PGC marker *Prdm1* promoter[51] to obtain *Tex10*$^{fl/+}$;*Prdm1*-Cre/+ mice, which were then mated with *Tex10*$^{fl/+}$ mice (Fig. S5a). We examined genotypes of liveborn pups from five litters, among which were 7 pups of Group1 (genotypes of *Tex10*$^{+/+}$, *Tex10*$^{fl/+}$, with or without Cre), 7 pups of Group2 (genotypes of *Tex10*$^{+/-}$ with or without Cre, and *Tex10*$^{fl/-}$ without Cre), and surprisingly no pups of *Tex10*$^{fl/-}$;*Prdm1*-Cre/+ genotype (Fig. S5a). Considering the low numbers of pups from each litter, we further examined 30 decidual swellings obtained at 12.5 *dpc* (*days post coitum*) from the same mating strategy. We found 19 blighted ova (Fig. S5b), 9 Group1 embryos, 2 Group2 embryos, and again no *Tex10*$^{fl/-}$; *Prdm1*-Cre/+ embryos (Fig. S5c). The Cre-mediated Tex10 was efficient with confirmed genotypes and reduced Tex10 protein levels to about 50% in *Tex10*$^{+/-}$ and *Tex10*$^{fl/-}$ compared to control (*Tex10*$^{fl/+}$ or *Tex10*$^{+/+}$) E12.5 embryos (Fig. S5d). The surprising lack of *Prdm1*-Cre excised *Tex10*$^{fl/-}$;*Prdm1*-Cre/+ embryos raised the question of how a PGC developmental defect, induced by Tex10 deficiency, would cause embryonic lethality at E12.5 (see Discussion).

https://doi.org/10.1038/s41467-025-57165-2

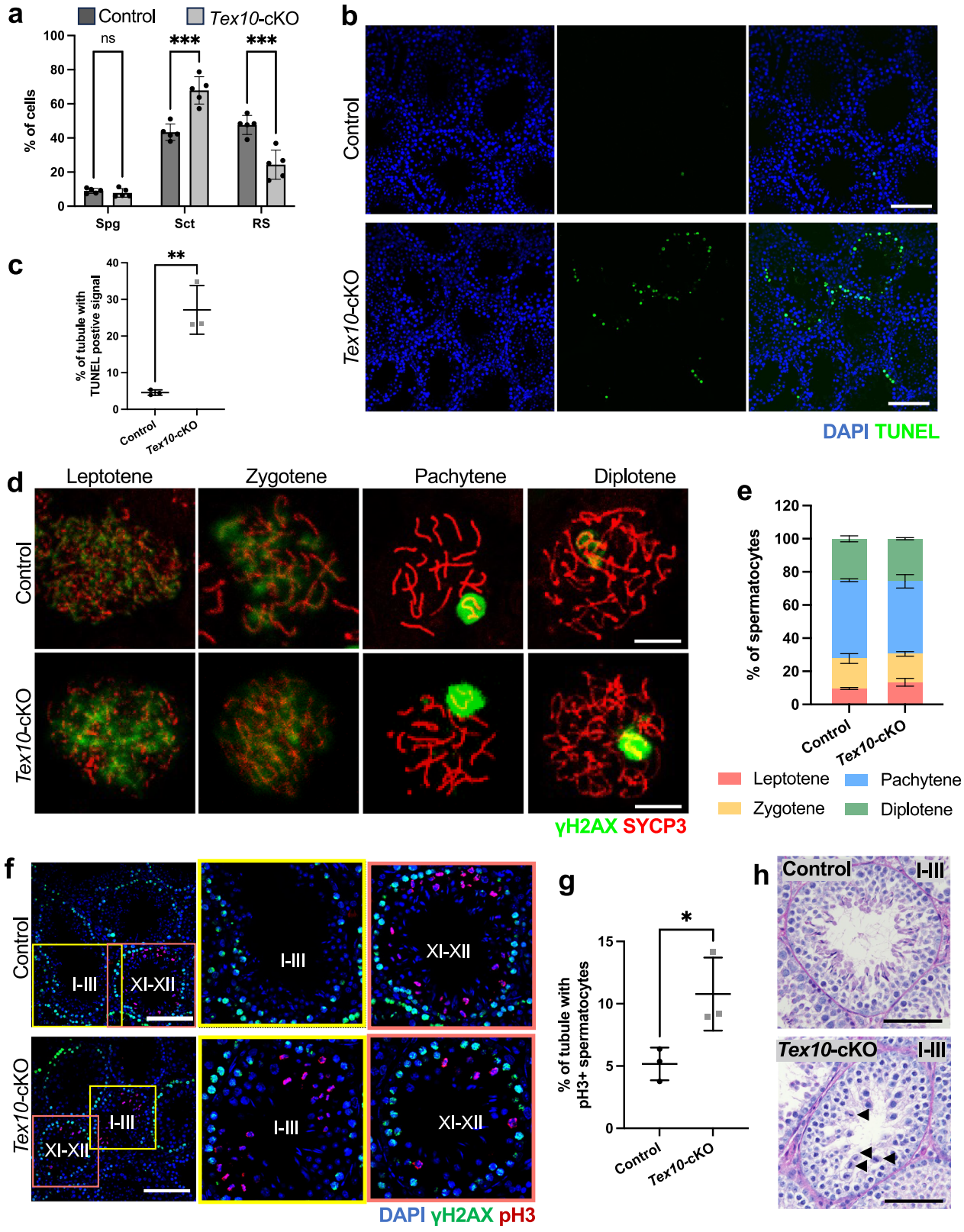

To obviate the embryonic lethality associated with *Prdm1*-Cre mediated Tex10 excision (Fig. S5a–d) and enable the dissection of the molecular mechanisms underlying Tex10 functions in PGC development, we turned to the well-established in vitro ESC-EpiLC-PGCLC differentiation system[25] (Fig. S1f and Methods). Owing to its requisite roles in the maintenance of ESCs[20], we set up the degron system[52] (Fig. 5a) to conditionally degrade Tex10 protein at specific periods during in vitro ESC-EpiLC-PGCLC differentiation. Using CRISPR targeting (Fig. 5a and Methods), we obtained and validated two Tex10 degron ESC clones (C1 and C2 in Fig. 5b). *Tex10* locus in these two clones was knocked in C-terminally with an in-frame HA-tagged $FKBP12^{F36V}$ expression cassette (Fig. 5a), resulting in the fusion protein ~12 kDa bigger than the wildtype Tex10 protein (Fig. 5b). Upon dTAG13 treatment, Tex10 is completely degraded within six hours (Fig. 5b).

Fig. 3 | Tex10 deficiency causes spermatocyte arrest at meiotic metaphase I and compromises round spermatid formation. a The percentage of spermatogonia (Spg), spermatocytes (Sct), and round spermatids (RS) cell populations in total cells from FACS. ($n = 5$ mice per condition.) Two-sided student's *t*-test. Error bars, mean ± SD. $p = 0.3798$ (ns for Spg), 0.0004 (*** for Sct), 0.0009 (*** for RS). Source data are provided as a Source Data file. **b** TUNEL staining (green) in control and *Tex10*-cKO adult testis sections. DAPI shows the nucleus. Scale bar, 100 µm. **c** The percentage of seminiferous tubules containing TUNEL positive signals from control and *Tex10*-cKO adult testis sections ($n = 3$ mice per condition). Two-sided student's *t*-test. Error bars, mean ± SD. $p = 0.0042$ (**). Source data are provided as a Source Data file. **d** Co-Staining of γH2AX (green) and SYCP1 (red) in nuclear surface spreads derived from control and *Tex10*-cKO adult testes. Scale bars, 20 µm. **e** The proportion of leptotene, zygotene, pachytene, and diplotene spermatocytes in control and *Tex10*-cKO adult testes ($n = 3$ mice per condition). **f** Co-staining of γH2AX (green) and pH3 (red) in control and *Tex10*-cKO adult testis sections. DAPI shows the nucleus. Scale bar, 100 µm. **g** The percentage of seminiferous tubules containing pH3 positive spermatocytes from control and *Tex10*-cKO adult testis sections ($n = 3$ mice per condition). Stages of the seminiferous epithelial cycle are indicated. Two-sided student's *t*-test. Error bars, mean ± SD. $p = 0.0391$ (*). Source data are provided as a Source Data file. **h** PAS staining of testes sections from control and *Tex10*-cKO adult mice. The arrowheads show the metaphase cells in seminiferous tubules (type I-III) of *Tex10*-cKO testes. Scale bar, 50 µm.

We then tested DMSO/dTAG13 treatment during the initial ESC-to-EpiLC (24 and 48 h) differentiation and embryoid body (EB) formation before adding cytokines to induce PGCLCs. Our data show that Tex10 depletion impairs EpiLC differentiation and EB formation (Fig. S5e, f). Following the in vitro PGC induction protocol[25], we compared the EB morphology of dTAG13-treated (Tex10 depletion) and DMSO-treated (control) cells during the differentiation time course of two, four, and six days (D2/4/6EBs) under PGCLC culture condition. We found that, while the control cell clusters exhibited typical smooth boundaries of EBs (D2/4/6EBs), the boundaries of **d**TAG13-treated D2/4/6EBs (**d**D2/4/6EBs) became non-smooth and dispersed into small patches (Fig. 5c). Immunostaining with the PGC markers[53] Sox2 and AP2γ showed that Tex10 depletion significantly decrease the PGCLC population in day 2 and day 6EBs (Fig. 5d, e). We further performed flow cytometry with SSEA1 and CD61, two typical PGC surface makers. We confirmed that the number of SSEA1/CD61 double-positive cells, i.e., PGCLCs, were significantly decreased at day 2 and day 6 upon Tex10 depletion (Fig. 5f, g), consistent with the reduced expression of Prdm1 (Fig. S5g). Finally, we demonstrated the reversible nature of Tex10 depletion by restoring its expression upon dTAG13 withdrawal after day one of PGCLC induction, which significantly increased PGCLC ratios and numbers compared to continuous depletion (i.e., no dTAG13 withdrawal) during the 6-day period (Fig. 5h, i), underscoring Tex10's critical role in PGCLC differentiation and cell survival.

Tex10 depletion disrupts PGC circuitry and promotes mesodermal lineage development

To understand how Tex10 promotes PGCLC differentiation, we investigated the transcriptional change induced by Tex10 depletion (Supplementary Data 6). A total of 1831 genes were upregulated in D2EBs vs. EpiLCs, among which 282 genes were downregulated by Tex10 depletion (Fig. 6a). GO analysis indicated that "stem cell population maintenance" and "germ cell development" were disrupted, manifested by the downregulation of the pluripotency genes such as *Klf4* and *Tcl1*, and germ cell development genes, including *Prdm1*, *Prdm14*, and *Kit*, as well as *Esrrb* and *Nanog* with dual functions in pluripotency and germ cell development (Figs. 6a and S6a). Of note, T/Brachyury, another crucial factor in mouse PGCLC specification, was relatively low in expression compared to the PGC marker Prdm1 and was not significantly affected by Tex10 depletion in our RNA-seq data (Supplementary Data 6) (see Discussion). On the other hand, 1278 genes were downregulated in D2EBs vs. EpiLCs, among which 326 genes were upregulated by Tex10 depletion. These genes are enriched in GO terms such as "cell adhesion" and "positive regulation of apoptotic process" (Figs. 6a and S6a). To examine the overall early effects of Tex10 depletion on the expression of pluripotency, PGC, and lineage differentiation genes, we conducted the activity analysis (see Methods for detail) on RNA-seq of **d**D2EBs vs. D2EBs. We found that pluripotency and PGC regulation activities decreased, while mesoderm and, to a lesser extent, endoderm development activities increased upon Tex10 depletion (Figs. 6b and S6b). Of note, PGC restrictor Otx2 was also increased upon Tex10 depletion (Fig. 6c).

Considering the mixed cell populations in EBs during PGCLC differentiation, we further performed bulk RNA-seq of purified **d**D2PGCLC vs. D2PGCLC and scRNA-seq of **d**D2EB vs. D2EB. A total of 187 genes were upregulated (e.g., *Cdkn1a*) and 466 genes were downregulated (e.g., *Prdm1*, *Nr5a2*) in **d**D2PGCLC vs. D2PGCLC (Fig. S6c and Supplementary Data 7). GO analysis showed that upregulated genes enriched in "positive regulation of apoptotic process" and "cell differentiation involved in embryonic placenta development" and downregulated genes enriched in "positive regulation of cell population proliferation" (Fig. S6d). Our scRNA-seq data revealed that Tex10 depletion led to a decreased PGCLC population (cluster 1) and increased extraembryonic-like cell populations (clusters 4 and 5) in day 2 EBs (Fig. 6d–f), concomitant with the downregulation of PGC development related genes and upregulation of extraembryonic-like cell development genes (Fig. 6g).

To examine a longer-term effect of Tex10 depletion on PGCLC differentiation, we treated the cells with dTAG13 (or DMSO) for 4 days, resulting in 2013 genes upregulated and 2494 genes downregulated in **d**D4EBs vs. D4EBs (Fig. S6e). Like the 2-day treatment, the 4-day treatment also compromised pluripotency and PGCLC differentiation, while lineage differentiation was enhanced, especially mesoderm development (Fig. S6f, g). Prdm1, Prdm14, and AP2γ are known to form the core PGC circuitry to initiate PGC-specific fate and repress somatic genes[10]. Expectedly, we found that *Prdm1* and *Prdm14* were significantly downregulated upon Tex10 depletion (Fig. S6h top panels). These two factors are also responsible for activating pluripotency genes[9]. Accordingly, among the consistently downregulated 162 genes upon two-day and four-day dTAG13 treatments, genes with functional GO terms such as "stem cell population maintenance" and "germ cell and oocyte development" were significantly enriched (Fig. S6h top panels). On the other hand, 172 genes were consistently upregulated and significantly enriched with functional GO terms on "apoptosis," "cell adhesion," and "heart development" in those 2-day and 4-day dTAG13-treated cells (Fig. S6h bottom panels). We further analyzed the expression of *Tex10*, *Prdm1*, *Prdm14*, and *Tfap2c* in ESCs, EpiLCs, PGCLCs, and EpiSCs based on the published microarray dataset[25]. All four factors' expression levels were increased from the EpiLC to PGCLC stage and reached the highest in PGCLCs compared to ESCs, EpiLCs, and EpiSCs (Fig. S6i). The co-upregulation of *Tex10* with known PGC specifier genes *Prdm1*, *Prdm14*, and *Tfap2c* further supports its potential role in PGC specification. Taken together, our data demonstrate that PGC development is positively regulated by Tex10, whose depletion leads to the disruption of the core PGC circuitry with a concomitant increase of apoptosis and somatic (mesoderm in particular) lineage development.

The Wnt signaling is hyperactivated by Tex10 depletion during PGCLC differentiation

The Wnt and BMP signaling pathways are well recognized for their roles in regulating the PGC circuitry[9]. Given that the core PGC circuitry is disrupted by Tex10 depletion, we asked whether these signaling pathways are also subject to Tex10 regulation. GSEA analysis of the Tex10 transcriptome revealed that the Wnt signaling pathway (NES = 1.48, *p*-value = 0.02), but not the BMP signaling pathway (NES = 0.77, *p*-value = 0.84), was activated by Tex10 depletion at the early PGCLC stage (Fig. 7a left two panels). Such an aberrant Wnt activation (i.e.,

hyperactivation) without a significant effect on BMP signaling was also observed in dD4EBs vs. D4EBs (Fig. 7a right two panels). Notably, it was recently reported that canonical BMP signaling is not cell-autonomously required to direct PGC-like differentiation[53]. This suggests that aberrant Wnt hyperactivation may play a major role in compromising the PGCLC differentiation of Tex10-depleted cells.

The Wnt signaling pathway is tightly regulated by intrinsic factors, such as Wnt ligands, receptors, and intracellular components, which can be modulated by extrinsic factors, including Wnt agonists, antagonists (e.g., Dkk, Sfrps), or small-molecule inhibitors at various levels[54]. Remarkably, the Wnt signaling positive regulators, such as *Wnt4* and *Wnt6*, were upregulated, whereas the Wnt signaling negative regulators, such as *Grb10*[55], *Sfrp1*[56], *Psmd3*[57–59], and *Psmd7*[60], were downregulated upon Tex10 depletion at both day 2 and 4 PGCLC stages (Fig. S7a). To establish a causal relationship between aberrant Wnt activation and compromised PGCLC differentiation, we added the

Fig. 4 | Tex10 regulates the Sct-to-RS transition through transcriptional control of meiosis and spermatic maturation genes. a Volcano plots depicting global transcriptomic changes in bulk RNA-seq of purified spermatogenic cells from control and *Tex10*-cKO adult testes. The numbers of upregulated and downregulated genes (|log2FC|> 0.5 & *p*-value < 0.05) in spermatogonia, MI/MII spermatocyte, and spermatid samples are indicated with red and blue text, respectively. **b** GSEA plots of cell-type-specific gene sets in bulk RNA-seq of purified spermatogenic cells from control and *Tex10*-cKO adult testes. **c** Heatmap for gene expression profiles of spermatogonia, meiotic recombination and kinetochore and microtubule in spermatocyte, and spermatid regulation markers in bulk RNA-seq of purified spermatogenic cells from control and *Tex10*-cKO adult testes. **d** Pseudotime analysis of scRNA-seq data from control and *Tex10*-cKO adult testes. The upper part shows the distribution of various subtypes, and the lower part displays the temporal order calculated by Monocle3. Smaller values represent earlier stages, while larger values represent later stages. **e** GO enrichment analysis of differentially expressed genes scRNA-seq data from control and *Tex10*-cKO spermatocytes (the top ten GO terms are shown). The size of each dot corresponds to the number of genes included in the respective GO term based on the set of differentially expressed genes. The horizontal axis gene ratio indicates the proportion of genes in the particular GO term relative to all differentially expressed genes. The dot color represents the significance of the corresponding GO term enrichment. P.adjust stands for the adjusted *P*-value, which is corrected by the Benjamini-Hochberg method.

Wnt inhibitor XAV939 (10 μM, the same concentration used in ref. 8) during PGCLC differentiation, which rescued the Tex10 depletion phenotypes by increasing the ratio of PGCLCs in live cells at days 2 and 4 (Figs. 7b, c, and S7b). As an alternative approach, we employed TCF/Lef:H2B-GFP reporter ESCs to read out the Wnt signaling response during PGCLC differentiation[53] (Fig. 7d). We found that, while GFP intensity was comparable between PGCLC (AP2γ+) and non-PGCLC (AP2γ-) populations before (except for D2EB) or after Tex10 depletion during the 6 days, it was significantly increased in both cell populations after Tex10 depletion at days 4 and 6 (Fig. 7e, f). Notably, non-PGCLCs are more sensitive in responding to Tex10 depletion with significantly higher reporter activity elevation (***$p < 0.001$) than PGCLCs (*$p < 0.05$; **$p < 0.01$) on day 4 and day 6 (Figs. 7f and S7c). As Wnt activation is often linked to enhanced proliferation of somatic cells in mesodermal and endodermal lineage[61], our studies suggest that Tex10 depletion may compromise PGC development through a combined action of aberrant activation of the Wnt signaling in both PGCs and non-PGCLCs during the differentiation process.

Tex10 overexpression promotes PGC development partly by restraining the Wnt signaling and suppressing somatic lineage programs

Given that Tex10 interacts with and regulates Nanog in mouse ESCs[20] and that Nanog acts as a potent inducer of PGC specification from ESC-derived EpiLCs[7], we next asked if Tex10 overexpression (OE) would promote PGC development. We first established two ESC clones transgenic for FLAG-tagged Tex10 and confirmed Tex10 OE relative to empty-vector (EV) control cells in EpiLCs (Fig. S8a). We then conducted the in vitro ESC-EpiLC-PGCLC differentiation and compared cellular morphology at different stages between OE and EV ESCs. Our results showed that the cellular morphology was similar across the day 2/4/6 time-course of differentiation (Figs. 8a and S8b) and that Tex10 OE increased the generation of PGCLCs at day 2 and significantly at day 6 but not the EpiLC stage, measured by SSEA1 and CD61 dual positivity (Figs. 8b and S8c). In line with these findings, immunostaining with PGC markers[53] Sox2 and AP2γ confirms that Tex10 OE significantly increased the PGCLC population in day 2 and day 6EBs (Fig. 8c, d). Accompanying the ectopic overexpression of Tex10 RNA (Figs. 8e and 9a) and protein (Figs. 8f and S8a), Nanog and Otx2 became upregulated and downregulated, respectively, during ESC-EpiLC-PGCLC differentiation, with a significant effect at the late PGCLC stage at both RNA and protein levels (Fig. 8e, f). However, Tex10 OE alone was insufficient to induce PGCLCs without the requisite cytokines (Fig. S8d–f).

To gain molecular insights into Tex10 OE in promoting in vitro PGC development, we investigated the time-course transcriptional changes during ESC-EpiLC-PGCLC differentiation (Supplementary Data 8 and 9). We first confirmed the ectopic OE of *Tex10* RNA at all stages (EpiLC, D2, D4, and D6 EBs, Fig. 9a). Core PGC circuitry genes (*Prdm1*, *Prdm14, Dppa3, Nanog*) and PGC regulator *Zfp296*[8] and *Nr5a2*[8] were maintained at relatively high expression levels throughout PGCLC stages compared to the EpiLC stage (Figs. 9b and S9a). Also, the expression of late-stage PGC markers, *Dazl* and *Kit*, increased greatly in the Tex10 OE at day 6 (Figs. 9b and S9b). Considering the potential competition between PGC fate and somatic lineage differentiation[51,62], we further utilized GSEA by focusing on somatic lineage and pluripotency genes. We found that pluripotency genes were significantly upregulated while mesoderm and ectoderm development genes were downregulated considerably upon Tex10 OE (Fig. 9c). In line with this, multilineage development genes were enriched in downregulated genes at the EpiLC (Fig. S9c), D2 (Fig. S9d), D4 (Fig. S9e), and D6 EBs (Fig. S9f) in Tex10 OE cells. On the other hand, the "stem cell population maintenance" GO term was enriched in upregulated genes at both D4 and D6 EBs (Fig. S9e, f). In addition, the GO term "DNA methylation" was also enriched in downregulated genes at EpiLC, D2, and D4 EBs (Fig. S9c–e) in Tex10 OE cells, in line with our previous finding of Tex10's role in DNA demethylation[20]. More importantly, "Wnt signaling" (especially canonical Wnt signaling) related GO terms were enriched in downregulated genes at D2, D4, and D6 EBs in Tex10 OE cells (Fig. S9d–f). Notably, the Wnt negative regulators *Psmd3 and Psmd7* were upregulated by Tex10 OE throughout the PGCLC differentiation stages from RNA-seq data of both bulk EBs (Fig. S9g) and purified PGCLCs (Fig. S9h).

To substantiate the connection between Tex10 functions in PGC development and Wnt signaling modulation, we compared publicly available RNA-seq data of known PGC regulators (Nr5a2, Hdac3, and Zfp296) and our Tex10 RNA-seq data in the context of Wnt signaling regulation and PGC development. We found that Tex10 depletion, *Nr5a2* KO[8], and *Hdac3* knockdown[63] datasets all showed Wnt signaling activation, whereas *Zfp296* KO[8] and Tex10 OE showed Wnt signaling inhibition (Fig. S9i). Based on existing data and prior knowledge that both aberrant Wnt activation and inhibition impair PGC specification[8], we created linear regression models to explore the correlation of Wnt signaling regulation with PGC regulation, pluripotency regulation, and lineage development under the context of Tex10, Hdac3, and Nr5a2 regulation, which shared similar regulatory patterns. We found that the GO term "positive regulation of Wnt signaling" is negatively correlated with PGC and pluripotency regulation (Fig. 9d top two panels) but positively associated with mesoderm development at the PGC specification stage (Fig. 9d bottom left panel). There was no apparent correlation between Wnt signaling and endoderm development (Fig. 9d bottom right panel). This mathematical model supports that the Wnt signaling is attenuated by Tex10 OE to promote PGC development while repressing somatic differentiation. However, possible functional interactions among Tex10 and these factors remain unknown. To experimentally test the results from these linear regression models, we treated the Tex10 OE cells with Wnt activator CHIR99021 (3 μM, the same concentration used in ref. 8). As predicted, the activation of Wnt signaling compromised the PGCLC formation induced by Tex10 OE (Fig. 9e). Together, we conclude that Tex10 overexpression restrains the Wnt signaling and suppresses somatic (the mesoderm lineage in particular) lineage programs in promoting pluripotency and PGC development.

https://doi.org/10.1038/s41467-025-57165-2

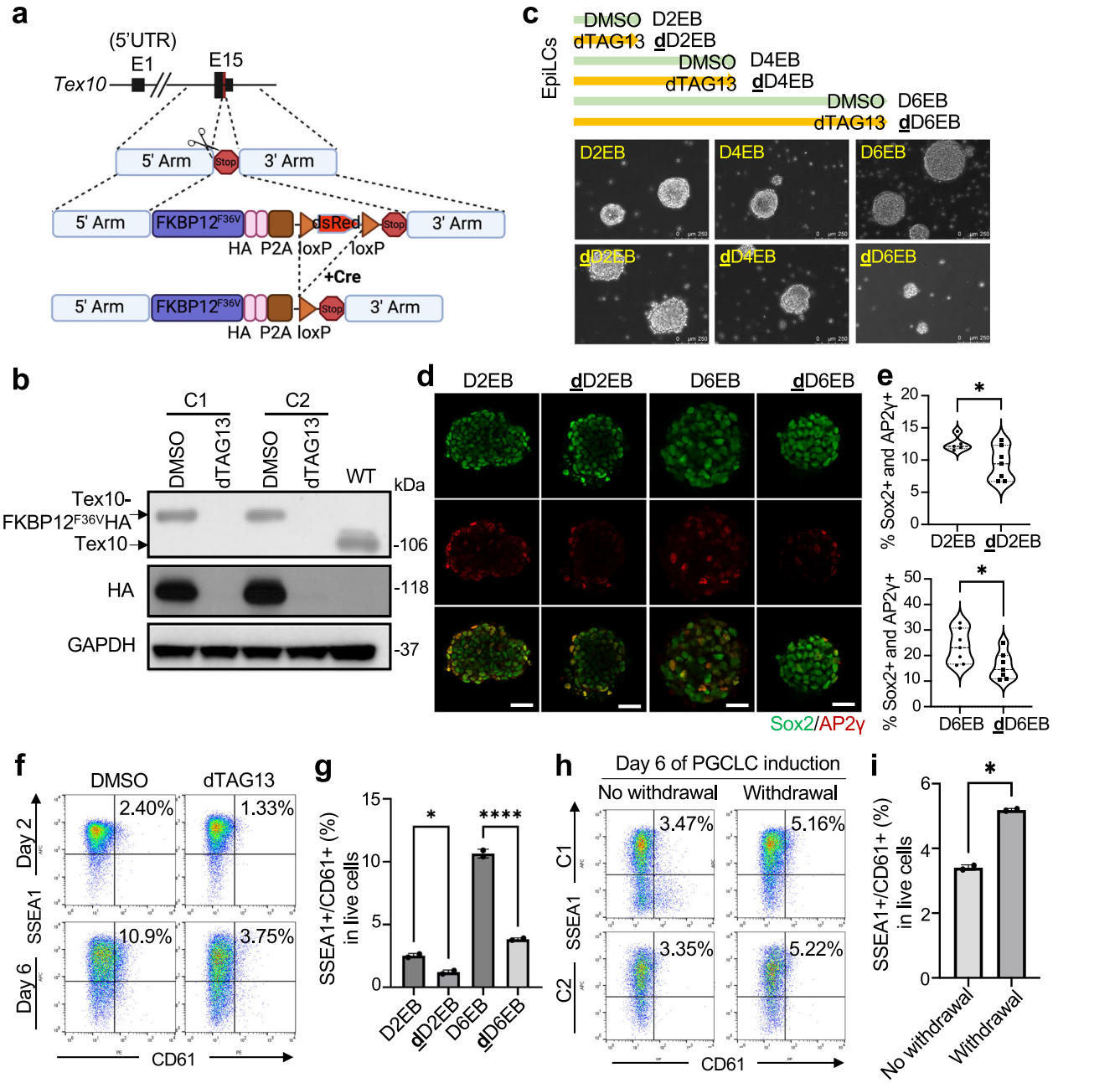

Fig. 5 | Loss of Tex10 compromises PGCLC specification efficiency. a Schematic of the Tex10 degron system. The Tex10 C terminus was knocked in with the FKBP12F36A and HA tag and the floxed dsRed cassette for selection using the CRISPR/Cas9 genome-editing approach. The Cre was further used to delete the dsRed element. **b** Western blot validation on two Tex10 degron ESC clones (C1 and C2). Tex10-HA-tagged FKBP12F36V protein with a size of around 118 kDa and the wildtype Tex10 protein with a size of 106 kDa were indicated. Source data are provided as a Source Data file. **c** Cellular morphology of embryoid bodies (EBs) treated with DMSO or dTAG13 during six days of in vitro PGCLC specification from EpiLCs. **d**, **e** Immunostaining (**d**) and quantification (**e**) of Sox2 and AP2γ in PGCLCs (Sox2+ and AP2γ+) and non-PGCLCs (Sox2− or AP2γ−) at day 2 and day 6EBs treated with DMSO or dTAG13. Each point represents a single cell. Scale bar, 20 μm. Quantification (**e**) was performed with a two-sided student's *t*-test. Error bars, mean ± SD. $p = 0.0358$ (* for top), 0.0320 (* for bottom). Source data are provided as a Source Data file. **f** Flow cytometry analysis of PGCLC specification efficiency using cell surface markers SSEA1 and CD61 with and without dTAG13 treatment. Percentages of double-positive (SSEA1+ and CD61+) cells are indicated on day 2 and day 6 of PGCLC induction from clone C1. **g** Quantification of double-positive (SSEA1+ and CD61+) percentages in live cells. Two cell clones, C1 and C2, were used as biological replicates ($n = 2$). One-way ANOVA test. Error bars, mean ± SD. $p = 0.0139$ (*), < 0.0001 (****). Source data are provided as a Source Data file. **h** Flow cytometry analysis of PGCLC specification efficiency using cell surface markers SSEA1 and CD61 with different treatments. Percentages of double positive (SSEA1+ and CD61+) cells are indicated at day 6 of PGCLC induction. No Withdrawal, depleting Tex10 throughout the six days of PGCLC induction; Withdrawal, depleting Tex10 only at day one of PGCLC induction, followed by transferring EBs into medium without dTAG13 to restore Tex10 expression. **i** Quantification of double-positive (SSEA1+ and CD61+) percentage in live cells. Two cell clones, C1 and C2, were used as biological replicates ($n = 2$). Two-sided student's *t*-test. Error bars, mean ± SD. $p = 0.0322$ (*). Source data are provided as a Source Data file.

The Wnt signaling inhibitors Psmd3/7 are direct transcriptional targets of Tex10 in PGCLCs and spermatogenic cells

To explore whether Tex10 directly targets and regulates the Wnt signaling regulatory genes, we performed ChIP-seq for Tex10 and H3K4me3 in D2EBs during PGCLC differentiation. We identified 4331 peaks (Supplementary Data 10) at the D2EBs, out of which ~70% peaks (3015/4331, corresponding to 2411 nearest genes) co-existed with the H3K4me3 histone mark (Fig. 10a and Supplementary Data 11),

https://doi.org/10.1038/s41467-025-57165-2

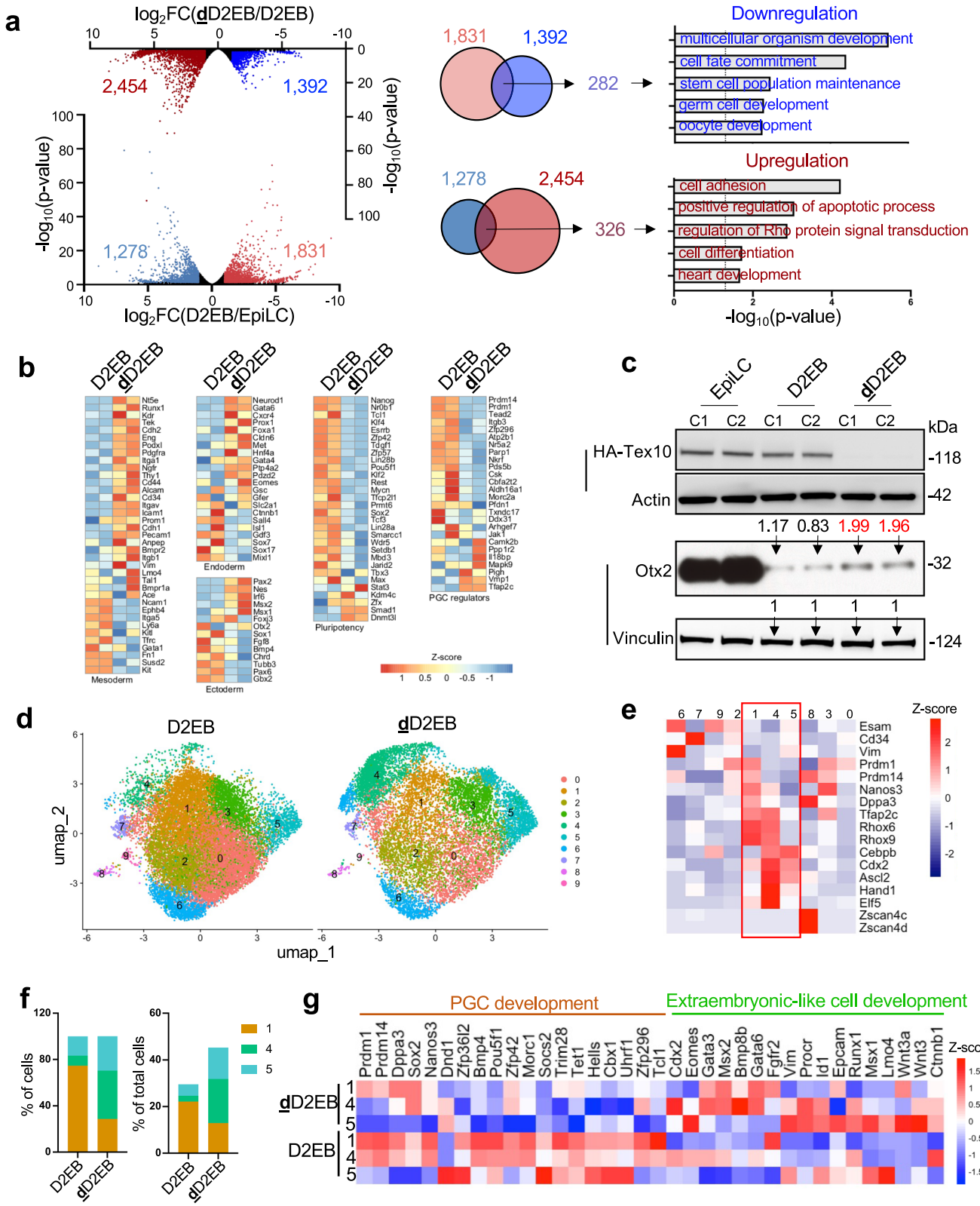

indicating that Tex10 binds to the potential promoter regions. We found 322 common genes after intersecting Tex10-bound/H3K4me3-marked genes ($n = 2411$) with genes that were downregulated ($n = 3076$, $\log_2FC < -0.5$ and p-value < 0.05) upon Tex10 depletion (Fig. 10b and Supplementary Data 12). GO analysis revealed that these genes were enriched with functional GO terms such as "negative regulation of apoptosis" (e.g., *Trim27* and *Tyro3*) and "negative regulation of Wnt signaling" (e.g., *Psmd3* and *Psmd7*) (Fig. 10c, d and Supplementary Data 13). On the other hand, we found 252 genes after intersecting Tex10-bound/H3K4me3-marked genes with genes that are upregulated ($n = 3241$, $\log_2FC > 0.5$ and p-value < 0.05, Supplementary Data 14) upon Tex10 depletion. The top enriched GO terms were related to cell proliferation, microvillus assembly, and negative regulation of TOR signaling (Fig. S10a, b and Supplementary Data 15); however, no Wnt signaling-related GO terms were enriched in the above 252 genes (Fig. S10a, c and Supplementary Data 15).

Fig. 6 | Molecular characterization of PGCLC specification upon Tex10 depletion. a Transcriptome profiling of bulk RNA-seq from EpiLC and whole EBs. Left: Volcano plots depicting the comparison of transcriptomic profiles of day 2 PGCLC (D2EB) vs. EpiLC stage (bottom volcano) and dTAG13-treated day 2 PGCLC (dD2EB) vs. control (D2EB; top volcano). Middle: Venn diagrams depicting the intersections between 1831 genes upregulated in D2EB vs. EpiLC and 1392 genes downregulated in dD2EB vs. D2EB, and between 1278 genes downregulated in D2EB vs. EpiLC and 2454 genes upregulated in dD2EB vs. D2EB (|log2FC|> 1 & *p*-value < 0.05). Right: enriched gene ontology biological processes are shown for the two overlapping gene sets in the middle panels. **b** Heatmaps for gene expression profiles of pluripotency, PGC, ectoderm, mesoderm, and endoderm regulation markers in D2EBs vs. dD2EBs. **c** Western blots of key PGC markers in EpiLCs, D2EBs, and dD2EBs. Data from two Tex10-degron clones (C1 & C2) are shown with dTAG13 added at the EpiLC stage, and Tex10 depletion ensued in dD2EBs. Quantification values for Otx2 relative to Vinculin are shown on top of bands for D2 and dD2 EB samples. Source data are provided as a Source Data file. **d**, **e** UMAP plot (**d**) of cell clusters identified within D2EBs and dD2EBs according to scRNA-seq data. Cluster identity (**e**) was determined by differential expression analysis between clusters and using specific tissue markers. PGCLC as cluster 1, extraembryonic-like cells as clusters 4 and 5 are highlighted with a red rectangle in **e**. **f** Cell proportion changes in D2EBs and dD2EBs according to scRNA-seq data. The left panel shows cell proportion in clusters 1, 4, and 5. The right panel shows the cell proportion of the total cells. **g** Heatmap for gene expression profiles related to PGC development (cluster 1) and extraembryonic-like cell development (clusters 4 and 5) from scRNA-seq of dD2EBs vs. D2EBs.

We validated the direct binding of Tex10 and H3K4me3 to the promoters of *Psmd3* and *Psmd7* by ChIP-qPCR (Fig. 10e). Psmd3/7 are components of the 19S proteasome subcomplex with reported roles in finetuning the Wnt/β-catenin signaling[57–60]. Particularly, Psmd7 is directly associated with the degradation of β-catenin from the proteasome[60]. We used two shRNAs to knock down Psmd7 (Fig. S10d, e), showing that Psmd7 knockdown phenocopied Tex10 depletion in compromising PGCLC generation (Fig. 10f). In contrast, the ectopic expression of Psmd7 partially rescued the PGCLC differentiation of Tex10-depleted (i.e., dTAG13-treated) cells (Figs. 10g and S10f, g). The partial rescue suggests the requirement of additional Tex10 targets (e.g., the other Wnt negative regulator Psmd3 or additional pathways) for Tex10's full function in PGC development. Together, these results demonstrate that Tex10 depletion may compromise PGC development through direct transcriptional repression of Wnt negative regulators such as Psmd3/7, resulting in aberrant activation of the Wnt signaling.

Next, we asked if a similar mechanism may underlie Tex10 functions in male germ cell development in vivo, given that hyperactivation and inhibition of Wnt signaling are known to impair spermatogenesis and germ cell development[13,64,65]. Indeed, our bulk RNA-seq analysis of the whole testis revealed a significant increase in canonical Wnt signaling and apoptosis in the *Tex10* cKO group (Fig. 10h). GSEA showed that genes upregulated by β-catenin accumulation (gene set ID: M5895[66,67]) were significantly enriched in *Tex10* cKO testes (Fig. 10i). Further, we observed a significant downregulation of Wnt negative regulators *Psmd3* and *Psmd7* (Fig. 10j) and upregulation of Wnt-associated genes such as *Fzd2* and *Ctnnb1* (Fig. S10h) in cKO testes compared to controls. Consistent with the TUNEL assay (Fig. 3b), apoptosis-related genes, including *Bax* and *Casp6*, were also elevated in the cKO group depletion (Fig. S10h). Analysis of scRNA-seq data from the whole testis showed a pronounced reduction in RS#2 and #3 clusters in cKO testes (Fig. S10i). GO enrichment of upregulated genes in RS#3 of cKO testes highlighted "positive regulation of Wnt signaling" (*p*-value < 0.05), though this was less significant than terms associated with meiosis and apoptosis (Fig. S10j). These findings suggest *Tex10* depletion activates Wnt signaling during spermatogenesis, particularly in round spermatid formation[13], and contributes to the observed abnormal sperm phenotypes. Together, our results indicate that Tex10 may regulate PGC and male germline development by finetuning Wnt signaling through transcriptional activation of its negative regulators (e.g., Psmd3/7).

Discussion

In this study, we identified Tex10 as a previously unappreciated player in controlling male germline development, including spermatogenesis in vivo and PGC induction from competent ESC-derived EpiLCs in vitro. Mechanistically, we found that Tex10 directly binds and transcriptionally activates Wnt negative regulators such as Psmd3/7 in maintaining the precise control of Wnt signaling for proper PGC development in vitro and possibly spermatogenesis in vivo (Figs. S10k left and S10l). Upon Tex10 depletion, the Wnt signaling is misregulated (i.e., hyperactivated), likely through direct transcriptional downregulation of its negative regulators such as Psmd3/7, resulting in compromised PGCLC formation and defective spermatogenesis (Figs. S10k right and S10l). On the other hand, Tex10 overexpression not only restrains the Wnt signaling but also restricts the somatic lineage programs while promoting pluripotency, leading to an overall effect of increased PGCLC induction/formation (Figs. 9, S9, and S10l). Although Wnt/β-catenin signaling plays a crucial role in all stages of spermatogenesis[12,13,68,69], it has remained controversial[64,65]. Balanced Wnt activity appears essential for normal spermatogenesis, as both overactivation and inhibition can lead to defects in male fertility[13,64,65]. Our findings thus add new insight into understanding Wnt signaling in spermatogenesis by revealing that Tex10 deficiency resulted in Wnt-related gene upregulation in the whole testis, especially in round spermatids, potentially compromising spermatid maturation. As Tex10 dysregulation is associated with human infertile patients[22] (Fig. S2j–l), our study thus provides a potential therapeutic target for treating male infertility.

T (also known as Brachyury) is a target gene of the Wnt/β-catenin signaling pathway[70] and a key PGC gene[71]. However, *T* was not significantly affected by Tex10 depletion in our RNA-seq data (Supplementary Data 6). The potential reason for T being detected with a low level in our experiments could be that the in vitro PGCLC differentiation system may not precisely mimic the signaling environment within the mouse embryo[53]. In vitro, as the majority of AP2γ$^-$ non-PGCLCs expressed Sox2 (Figs. 5d and 8c), they likely represent a pluripotent EpiLC or earlier PGCLC state and thus do not mirror the in vivo PGC niche that comprises extraembryonic mesoderm[53]. Alternatively, we found that *T* was not a direct binding target of Tex10, whereas the two Wnt negative regulators Psmd3 and Psmd7 were direct binding targets of Tex10 (Fig. 10d, e). The expression levels of these two genes are significantly affected by Tex10 depletion and overexpression (Figs. S7a and S9g, h). Therefore, we speculate that the regulating effect of Tex10 on Wnt signaling is more likely due to its impact on Wnt negative regulators rather than on *T*. However, future studies are needed to distinguish this regulatory effect in PGCLCs (or spermatogenic cells in the testis) from non-PGCLCs (or somatic cells in the testis).

Pluripotency reactivation is a notable feature of PGC specification[9,10]. For core pluripotency genes Nanog, Oct4, and Sox2[72,73], conditional deletion of Sox2[16] or Oct4[15] and induced knockdown of Nanog result in PGC death/apoptosis[74]. In addition, deleting the Nanog target gene Esrrb reduces PGC numbers in vivo[75]. Along this line, we found that depletion of Tex10, an interaction partner of Nanog, Oct4, and Sox2[20], induces apoptosis during the in vitro PGC induction (Figs. 6a and S6a, h) and in vivo germline development (Fig. 3b). Conversely, and like Nanog[7], ectopic expression of Tex10 greatly enhances PGC induction from competent EpiLCs. Taken

https://doi.org/10.1038/s41467-025-57165-2

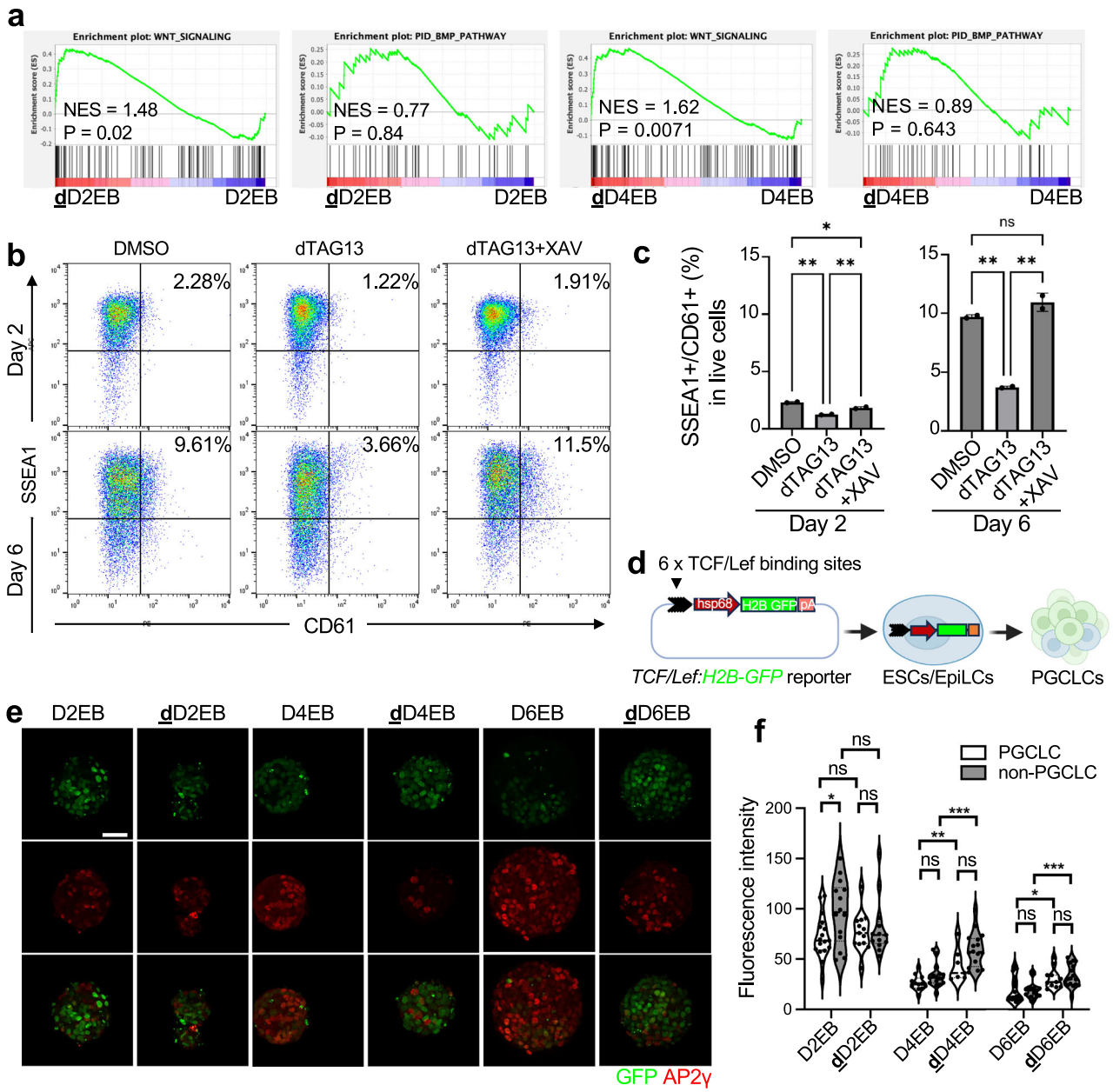

Fig. 7 | Tex10 depletion causes the Wnt signaling hyperactivation during PGCLC differentiation. a GSEA analysis showing Wnt signaling but not BMP signaling is activated by Tex10 depletion at day 2 and day 4 EBs. **b** Flow cytometry analysis of PGCLC specification efficiency using cell surface markers SSEA1 and CD61. Percentages of double positive (SSEA1+ and CD61+) cells are indicated at day 2 and day 6 of PGCLC induction for clone C1. **c** Quantification of double-positive (SSEA1+ and CD61+) percentage in live cells. Two cell clones, C1 and C2, were used as biological replicates ($n = 2$). One-way ANOVA test. Error bars, mean ± SD. $p = 0.0125$ (Day2 *), 0.0012 (Day2 left **), 0.0067 (Day2 right **), 0.1462 (Day6 ns), 0.0020 (Day6 left **), 0.0012 (Day6 right **). Source data are provided as a Source Data file. **d** The TCF/Lef:H2B-GFP reporter construct was used in this study[97]. Tandem copies of Tcf/Lef binding motifs were inserted upstream from a core hsp68 promoter driving expression of H2B: GFP, which read out canonical Wnt signaling activity during PGCLC in vitro differentiation. Created in BioRender. Wang, J. (2025) https://BioRender.com/n34e702. **e** Representative image of day 2, 4, and 6EBs induction from TCF/Lef:H2B-GFP reporter EpiLCs. GFP (green) shows the Wnt signaling activity. Scale bar, 20 μm. **f** Quantitative immunofluorescence of signaling responses in PGCLCs (AP2γ+) and non-PGCLCs (AP2γ−) at day 2, day 4, and day 6EBs. Each point represents a single cell. One-way ANOVA test. Error bars, mean ± SD. $p < 0.001$ (***), $p < 0.01$ (**), $p < 0.05$ (*), and $p > 0.05$ (ns). Source data are provided as a Source Data file.

together, our data indicate the dual roles of the core ESC transcription factors in regulating both stem cell pluripotency and germ cell development and suggest that disrupting the core pluripotency network would lead to PGC loss. However, early embryonic lethality and the loss of stem cell maintenance are often associated with the loss of functions of these factors (e.g., Nanog[76], Oct4[77], Sox2[78], and Tex10[20]); understanding their functional roles in germline development often requires an inducible or conditional KD/KO system. In this regard, our newly developed Tex10 degron ESCs and cKO mouse models enabled us to uncover the critical roles of Tex10 in PGC development and spermatogenesis in this study.

Despite its wide use in studying in vivo PGC development, the *Prdm1*-Cre was reported to be active also on primitive endoderm (PrE) at E6.75-9.0[79], which overlaps with mouse PGC specification (E6.25-8) and migration (E8.5-10.5) stages in vivo[80]. The yolk sac, which develops from the PrE, provides gas and nutrition exchange between the developing embryo and the mother[81]. Considering the apoptosis effect induced by Tex10 depletion from our in vitro study (Figs. 6a and S6a, f)

https://doi.org/10.1038/s41467-025-57165-2

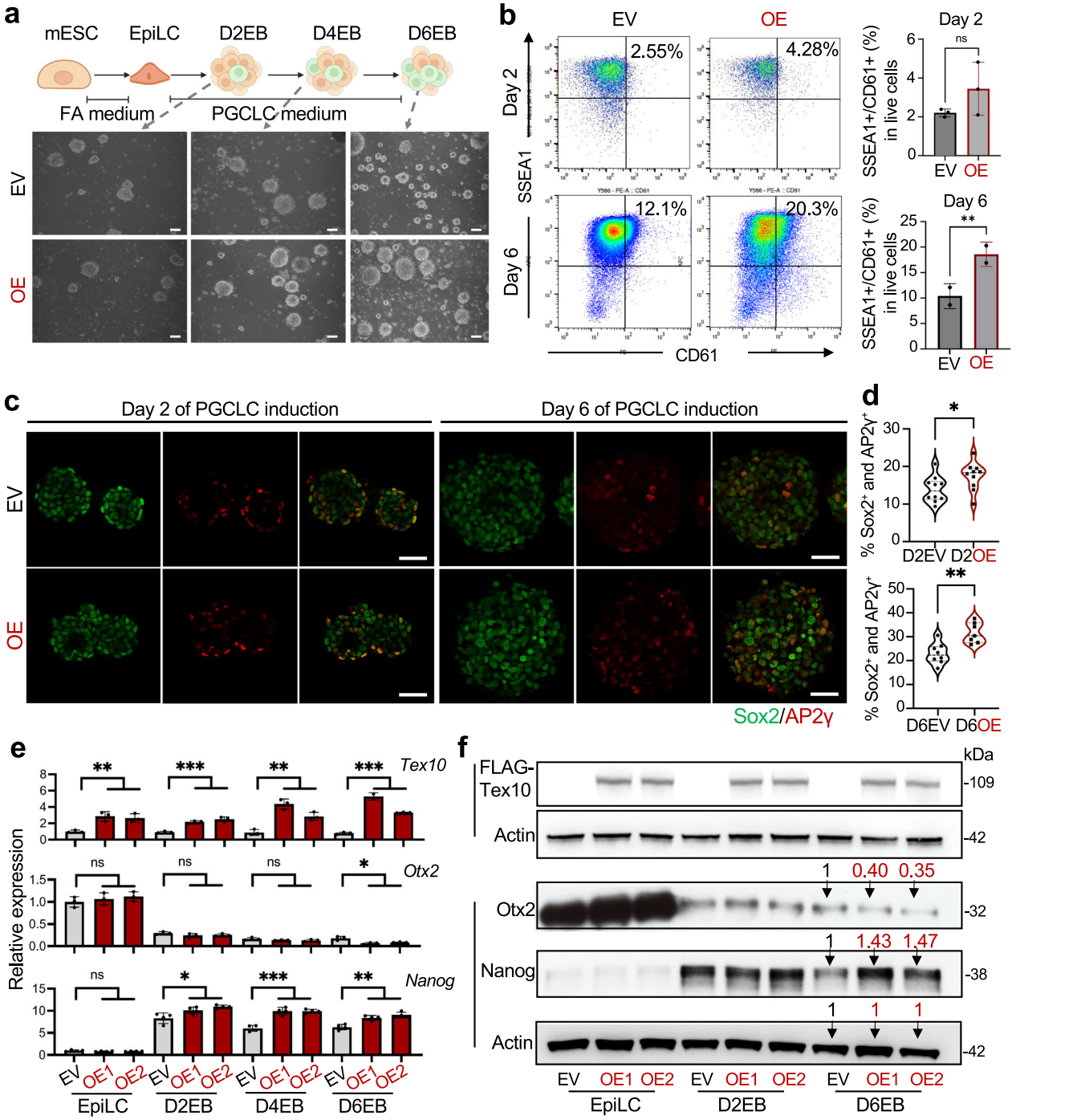

Fig. 8 | Tex10 overexpression enhances PGCLC specification efficiency. **a** Cellular morphology of Tex10 overexpression (OE) vs. control (Empty vector, EV) EBs at day 2, day 4, and day 6. Scale bar, 100 µm. Top illustration was created in BioRender. Wang, J. (2025) https://BioRender.com/n34e702. **b** Flow cytometry analysis of PGCLC specification efficiency at day 2 and day 6 using markers SSEA1 and CD61(left panel). Percentages of double positive (SSEA1+ and CD61+) cells in live cells are indicated at day 2 (top of right panel) and day 6 (bottom of right panel) of PGCLC induction. Two cell clones, OE1 and OE2, were used as biological replicates ($n = 2$). Two-sided student's t-test. Error bars, mean ± SD. $p = 0.2264$ (ns), 0.0019 (**). Source data are provided as a Source Data file. **c**, **d** Immunostaining (**c**) and quantification (**d**) of Sox2 and AP2γ in PGCLCs (Sox2+ and AP2γ+) and non-PGCLCs (Sox2− or AP2γ−) at day 2 and day 6 Tex10 overexpression (OE) and control (EV) EBs. Each point represents a single cell. Scale bar, 20 µm. Quantification (**d**) was performed with a two-sided student's t-test. Error bars, mean ± SD. $p = 0.0424$ (*), 0.0018 (**). Source data are provided as a Source Data file. **e** Quantitative RT-PCR analysis of *Tex10*, *Otx2*, and *Nanog* expression during the transition from EpiLCs to D2, D4, and D6 EBs. Two cell clones, OE1 and OE2, were used as biological replicates ($n = 2$, each clone with one or two technical replicates). One-way ANOVA test. Error bars, mean ± SD. $p < 0.001$ (***), $p < 0.01$ (**), $p < 0.05$ (*), and $p > 0.05$ (ns). Source data are provided as a Source Data file. **f** Western blot analysis of FLAG-Tex10, Otx2, and Nanog expression during the transition from EpiLCs to D2, D4, and D6 EBs. Quantification values for Otx2 and Nanog relative to Actin are shown on the top of bands for D6EB samples. Source data are provided as a Source Data file.

https://doi.org/10.1038/s41467-025-57165-2

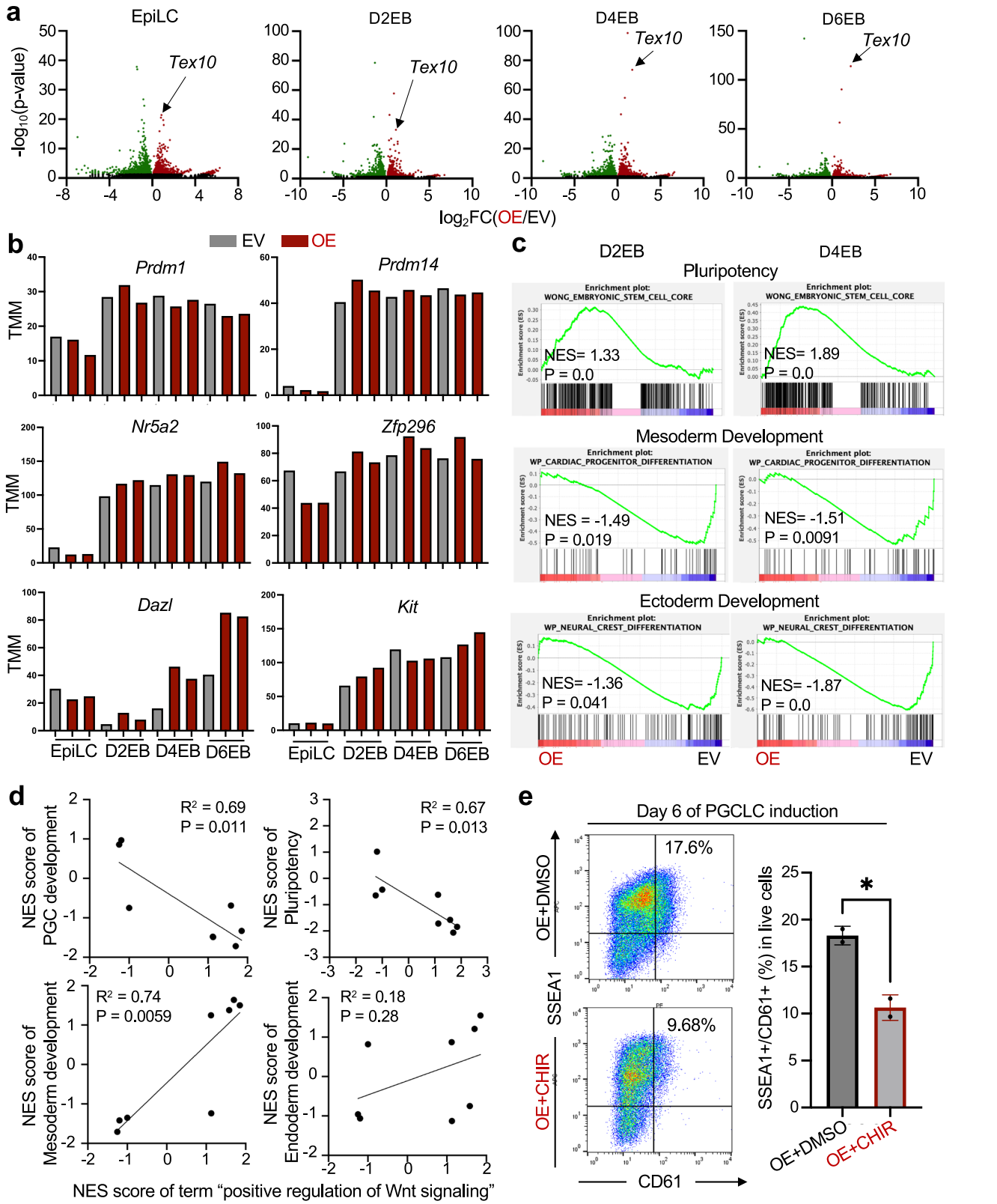

Fig. 9 | Tex10 overexpression restricts the Wnt signaling and somatic lineage programs in promoting pluripotency and PGC development. a Volcano plots depicting global transcriptomic changes upon Tex10 OE at EpiLCs, and D2, D4, D6 EBs. **b** Bar plots showing expression changes of representative PGC regulators upon Tex10 OE during the transition from EpiLCs to D6 EBs. **c** GSEA analysis of the effects of Tex10 OE on pluripotency, mesoderm, and ectoderm development at D2 and D4 EBs. **d** Regression models exploring the correlation between NESs (normalized enrichment scores) of the positive regulation of Wnt signaling and PGC development, pluripotency regulation, mesoderm, and endoderm development. **e** Flow cytometry analysis of the effect of Wnt activator (CHIR: CHIR99021) on PGCLC specification efficiency in Tex10 OE cells. The percentages of double positive (SSEA1+ and CD61+) cells are indicated on day 6 of PGCLC induction (left). The quantification of double-positive percentages in live cells is shown in the bar plots (right). Two cell clones, OE1 and OE2, were used as biological replicates ($n = 2$). Two-sided student's t-test. Error bars, mean ± SD. $p = 0.0232$ (*). Source data are provided as a Source Data file.

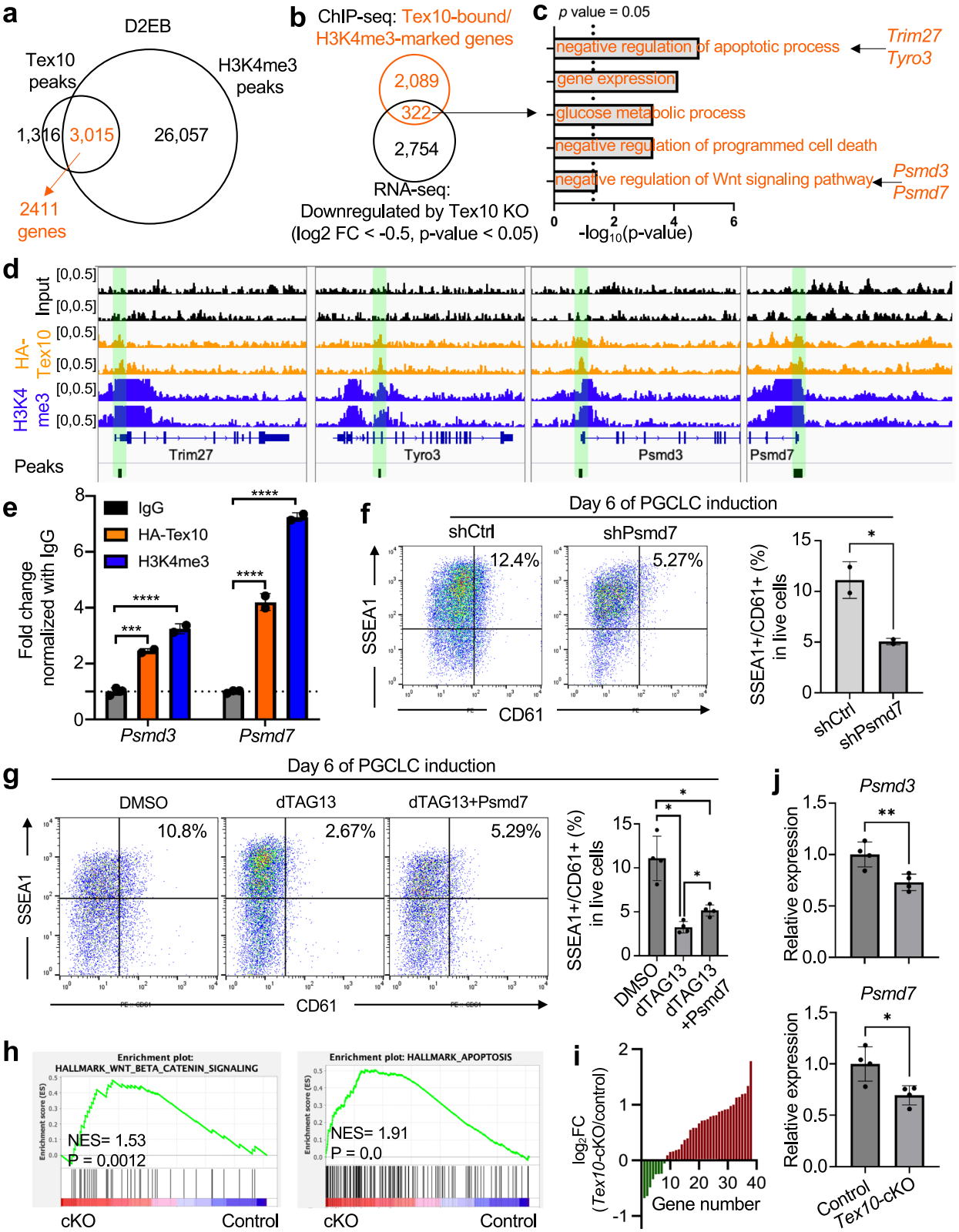

and detectable expression of *Tex10* in extraembryonic tissues[82,83] (Fig. 1a), we speculated that the unintended Tex10 knockout in extraembryonic tissues (yolk sac and PrE) might have compromised the embryogenesis at E6.75-9.0, precluding the use of this Cre line in our study.

Finally, epigenetic reprogramming enables the transition from PGC to gonocyte[84]; it remains to be determined how extensive genome reprogramming and alteration of DNA methylation and histone modification may contribute to Tex10 transcriptional functions. The enrichment of GO term "DNA methylation" in downregulated genes at EpiLC and D2-4 PGCLC stages upon Tex10 OE (Fig. S9c–e) is particularly intriguing, considering that PGC specification is anti-correlated with DNA methylation[85] and that Tex10 can bridge the core pluripotency factor Sox2 with DNA hydroxylase Tet1 for the DNA hypomethylation status of the super-enhancers associated with pluripotency genes[20]. Future studies to map the Tex10 interactome in

Fig. 10 | The Wnt negative regulators Psmd3/7 are direct targets of Tex10 whose downregulation by Tex10 depletion compromises PGCLC specification and spermatogenesis. a Venn diagram showing the overlap between Tex10 and H3K4me3 ChIP-seq peaks at the D2PGCLC stage. **b**, **c** Venn diagram showing the intersection between Tex10-bound/H3K4me3-marked genes and genes downregulated upon Tex10 depletion (**b**) and gene ontology biological processes enriched in the overlapping 322 genes (**c**). **d** Genome browser tracks of Tex10 and H3K4me3 ChIP-seq signals near Trim27, Tyro3, Psmd3, and Psmd7 gene loci in D2EBs. Green shaded regions indicate the Tex10 peaks. **e** ChIP-qPCR validation of Tex10 binding and H3K4me3 marks at the promoter regions of Psmd3 and Psmd7. The Tex10 ChIP experiment was performed in D2EBs with an anti-HA tag antibody, and IgG served as a negative control. Two cell clones, C1 and C2, were used as biological replicates ($n = 2$, each clone with one or two technical replicates). One-way ANOVA test. Error bars, mean ± SD. $p = 0.0005$ (***) and $p < 0.0001$(****). Source data are provided as a Source Data file. **f**, **g** Flow cytometry analysis of PGCLC induction efficiency using cell surface markers SSEA1 and CD61. Percentages of double positive (SSEA1+ and CD61+) cells are shown on day 6 of PGCLC induction for control shRNA (shCtrl) and Psmd7 shRNA (sh*Psmd7*) (**f**) and for treatments with DMSO, dTAG13, and dTAG13 plus ectopic Psmd7 (dTAG13+Psmd7) (**g**). Bar plots show the quantification of double-positive percentages in live cells with $n = 2$ biological replicates for the two control shRNAs vs. two sh*Psmd7* (**f**) or the two cell clones C1 and C2 (**g**). Two-sided student's *t*-test. Error bars, mean ± SD. $p < 0.05$ (*). Source data are provided as a Source Data file. **h** GSEA plots of the Wnt/β-catenin signaling and apoptosis gene sets in bulk RNA-seq of whole testes from adult control and *Tex10*-cKO mice. **i** Wnt/β-catenin signaling is hyperactivated upon Tex10 depletion in mouse testes. The genes ($n = 42$) from the MSigDB term "upregulated by the accumulation of β-catenin" were intersected with our bulk RNA-seq of whole testis data (38 genes found). The regulatory effects of *Tex10* cKO (upregulated in red and downregulated in green) on these genes are shown as bar plots. **j** Quantitative RT-PCR analysis of *Psmd3* and *Psmd7* showing their downregulation in *Tex10*-cKO relative to control testes ($n = 4$ mice per condition). Two-sided student's *t*-test. Error bars, mean ± SD. $p = 0.0098$ (**), 0.0186 (*). Source data are provided as a Source Data file.

PGCs will reveal its potential physical and functional interactions with other PGC specifiers, such as Oct4[15] and Nanog[7], and epigenetic regulators, such as Tet family proteins[86]. This will unravel the transcriptional and epigenetic roles of Tex10 in PGC specification and male germline development.

Methods

Animals

As the Tex10 conventional knockout mice model is early embryonic lethal[20], we generated the Tex10 conditional knockout mice to evaluate its function in germ cell development. Tex10 is a gene with multiple exons and has a few splicing isoforms in the first three exons. To preserve the internal initiation site and minimize the chance of downstream in-frame methionine codons being used as translational start and producing a truncated protein, we only considered floxing exon 5 and later exons. Given convenience for genotyping with only 113 bp, exon 5 was chosen to be excised to disrupt the Tex10 gene functionally. Accordingly, two loxP sites were inserted to flank the exon 5. Such deletion was predicted to produce transcripts with premature stop codons and activate nonsense-mediated mRNA decay, thus leading to Tex10 knockout. However, as loxP is only 34 bp in length, distinguishing the wildtype and inserted allele is not easy. To overcome this hurdle, a BamHI site was also added to loxP. Then, Cre-Lox recombination was used to delete the DNA fragment between these two loxP sites (Fig. S2a).

CRISPR/Cas9 targeting reagents for Tex10 conditional knockout (KO) founder lines were designed, generated, and confirmed or validated at Genome Engineering & iPSC Center (GEiC) at Washington University (WashU St. Louis, MO). These reagents were delivered to the Mouse Genetics and Gene Targeting (MGGT) core in Icahn School of Medicine at Mount Sinai for zygote injection to generate CRISPR babies, among which founder mice were identified. By co-injecting Cas9 plasmid, validated gRNAs, and single-strand oligonucleotide donor DNAs (ssODN) into fertilized eggs from C57BL/6 N mice, we obtained 66 mice (one died shortly after being born) for next-gene sequencing (NGS service provided by WashU St. Louis, MO). We identified three mice with correct loxP-BamHI sites in both introns 4 and 5 of the same allele, namely founders #45 (male), #46 (male), and #53 (female). To ensure the loxP-BamHI sites can be transmitted to the next generation, the three founders were mated with wildtype C57BL/6 N mice, and resulting pups were genotyped for both 5′ and 3′ loxP-BamHI sites, respectively. Fragments containing the two loxP-BamHI sites were amplified by F1 ~ F3 and sequenced again for verification. The pups from founder #45 (male) had the correct loxP-BamHI sites and intact introns 4 and 5, which were used for the subsequent studies. Three primers were designed for genotyping, namely F1, F2, and F3 (Fig. S2a and Supplementary Table 1). The deletion by certain Cre strains produced the "−" band at 360 bp from the 470-bp "fl" loxP band, and the wildtype "+" was at 430 bp (Fig. S2a). The gRNAs sequences for intron 4: 5′-cctatgggctgggccctacataa-3′ and intron 5: 5′-ccataagtgtggcacctgtgtgc-3′.

All animal experiments were conducted according to institutional guidelines for animal welfare and approved by Columbia University's Institutional Animal Care and Use Committee (IACUC Protocols#AC-AACB2706 and AC-AABT8666).

Construction of the Tex10 Degron ESC lines

The male J1 mouse ESCs (mESCs) were maintained in ES medium containing 80% high-glucose DMEM, 15% fetal bovine serum (FBS, Corning, 35015CV), 1% nucleoside mix, 100 μM nonessential amino acids, 50 U/mL penicillin/streptomycin, 0.1 mM 2-mercaptoethanol, 2 mM L-glutamine, and homemade recombinant leukemia inhibitory factor (LIF).

The 5′ arm and 3′arm of *Tex10* C-terminal were cloned from the genomic DNA of J1 mESCs, and FKBP-V-2xHA-P2A-BFP was cloned from pAW63.YY1.FKBP.knock-in.BFP plasmid (Addgene plasmid #104371). Then, Gibson cloning was performed to connect the above three fragments. The PCR product from Gibson assembly was purified and cloned into pJet1.2 plasmid (CloneJET PCR Cloning Kit, Thermo Fisher Scientific). Then, the loxP-dsRed-loxP fragment was cloned from pMSCV-loxP-dsRed-loxP-3xHA-Puro-WPRE (Addgene plasmid #32703). The loxP-dsRed-loxP fragment and the above modified pJet1.2 plasmid were digested with restriction enzymes AgeI (NEB, R0552S) and PacI (NEB, R0547S) and then ligated using T4 DNA ligase (NEB, M0202S) to get pAW63-Tex10 plasmid. The Tex10 guide RNA sequence was inserted into the PX330-puro plasmid (Addgene plasmid #62988) to get the PX330-Tex10 plasmid.

J1 mESCs were transfected with pAW63-Tex10 and PX330-Tex10 plasmids using Lipofectamine 3000 (Thermo Fisher Scientific, L3000001) according to the manufacturer's manual, followed by drug selection using puromycin (1 μg/mL) for three days. The selected cells were transfected with the pPyCAG-CreERT2-ires-Puro plasmid, modified from pPyCAG-Cre::ERT2-IRES-BSD (Addgene plasmid #48760) by changing blasticidin-resistance gene to puromycin-resistance gene, and then treated with 4-hydroxytamoxifen (Sigma, H7904) to delete the dsRed fragment. Clones with no fluorescence were picked and expanded. Expanded clones were treated with or without dTAG13 (500 nM, Toronto Research Chemicals, D710020) and compared with wildtype J1 mESCs for Tex10 expression. The size difference of Tex10 proteins between successful clones and wildtype is around 12 kDa, which is the size of HA-tagged $FKBP12^{F36V}$, and dTAG13 treatment (500 nM) fully degraded the Tex10 protein. Two clones were validated and used for the following in vitro PGCLC specification experiments. The primers used are listed in Supplementary Table 1.

Induction of EpiLCs and PGCLCs

EpiLCs and PGCLCs induction were conducted following the published protocol[25]. Briefly, mESCs were cultured in 2i (3 μM CHIR99021 and 1 μM PD0325901) plus LIF medium for seven days to achieve the naive pluripotency state. Then, the medium was replaced with FA (12 ng/mL bFGF and 20 ng/mL Activin A) medium for two days to obtain EpiLCs. After that, 5×10^4 EpiLCs for one well of a 24-well plate or 4×10^3 EpiLCs for one well of a 96-well plate were used for PGCLC induction. The plates were coated with Pluronic® F-127 (Sigma, 9003116) to make it low attachment, thus preventing cell adhesion on the bottom of wells[87]. PGCLC medium (500 ng/mL BMP4, LIF, 100 ng/mL SCF, 500 ng/mL BMP8b, and 50 ng/mL EGF) was used to induce PGCLC formation for two, four, and six days, and cells were subjected to immunostaining or flow cytometry to detect specification efficiency. Compared with the previous protocol[25], we used the same set of cytokines. The only minor variation was that we used the 24-well plates with the F-127 coating to obtain enough material for downstream western blot analysis.

FACS

The mouse testicular cell suspension, Hoechst dye staining, and flow cytometric analysis were conducted following the published protocol[48]. Testes isolated from 8-week-old male mice were dissected, and tunica albuginea was removed in PBS. Seminiferous tubules were dispersed with tweezers and incubated with 7 ml collagenase type IV (290 U/ml, Gibco, 17104-019) for 10 min at 37 °C with gentle agitation (250 rpm) in 15 ml centrifuge tubes. The tubules were sedimented naturally for 2 min, and 6 ml suspension was discarded. Four ml DPBS (Corning, 21031CV), 5 ml 0.25% Trypsin-EDTA (Gibco, 25200056), and 10 μg/ml DNase I ((Invitrogen, 18068015) was added for digestion for 8 min at 37 °C. Six hundred μL FBS was used to end digestion. Cells were filtered with 70 μm (Falcon, 352350) cell strainer and treated with 100 μg Hoechst (Thermo Fisher Scientific, H3570) for 20 min at room temperature (RT). Next, these pre-stained cells were centrifuged and resuspended with DMEM supplemented with 10% FBS and 10 μg/ml DNase I. Cells were stained with 6 μg Hoechst per million cells for 30 min at RT. Finally, stained cells were filtered with a cell strainer (Falcon, 352235) and put on ice until flow cytometric analysis. For PGCLCs analysis, EBs at the indicated time were dissociated with 0.05% Trypsin-EDTA (Gibco, 25200054) and washed with DMEM containing 10% FBS. After that, Cells were stained with PE anti-mouse/rat CD61 (1:200, Biolegend, 104307) and Alexa Fluorβ 647 anti-mouse/human SSEA1 antibodies (1:50, Biolegend; 125608) for 30 min on ice. Cells were then washed with 1×PBS containing 0.1% BSA, and large clumps of cells were removed using a cell strainer (Falcon™ 352235). All samples were analyzed using LSRII flow cytometry in Columbia University's flow core facility. FACS data were analyzed using FlowJo v10.6.2.

Histological analysis

Testes and epididymis cauda isolated from 8-week-old male mice and ovaries from 28-day-old female mice were dissected and fixed in 4% paraformaldehyde (PFA, Thermo Fisher Scientific, 28908) at 4 °C overnight. Then, tissues were dehydrated through a series of grade ethanol, embedded in paraffin, and sectioned at 5 μm. After deparaffinization and hydration, sections were stained with periodic acid Schiff (PAS, Sigma, 395B) or hematoxylin and eosin (H&E, Sigma) following standard protocols. Images were acquired with the Leica (DM4B) microscope.

Chromosome spreads

Testes isolated from 8-week-old male mice were dissected, and spermatocytes were collected by FACS as described above. Briefly, a 50 μL aliquot of sorted cells was mixed with 50 μL hypotonic extraction buffer (30 mM Tris-HCl pH 8.5, 50 mM sucrose, 17 mM citric acid, 5 mM EDTA) for 30 min at room temperature. After centrifuge, cells were resuspended in 100 mM sucrose/H_2O. Twenty μL cell suspensions were dropped onto adhesion microscope slides (Fisher Scientific, 361044950) spread with 20 μL fixation buffer (1% PFA and 0.15% Triton X-100) from a high place, fixed for 3 h at room temperature, and air-dried for 1 h in room temperature. Slides were washed three times in PBS before immunostaining experiments.

Immunofluorescence and TUNEL staining

Testes isolated from 8-week-old male mice and ovaries isolated from 28-day-old female mice were fixed in 4% PFA at 4 °C overnight, embedded in paraffin, and sectioned at 5 μm. The sections were dewaxed, rehydrated, and subjected to antigen retrieval. After blocking with 10% normal donkey serum, the sections were incubated with primary antibodies anti-PLZF (1:50, mouse IgG, Santa Cruz, sc-28319), anti-DDX4 (1:100, rabbit IgG, Abcam, ab196708), anti-Tex10 (1:100, rabbit IgG, Thermo Fisher Scientific, 720257), anti-β-galactosidase (1:500, mouse IgG, Thermo Fisher Scientific, Z3781), anti-Sox9 (1:1000, rabbit IgG, Sigma-Aldrich, AB5535), anti-Phospho-Histone H3 (Ser10) (1:100, rabbit IgG, Thermo Fisher Scientific, MA5-15220) at 4 °C overnight. After washing three times with PBST (PBS with 0.1% Tween-20), slides were incubated with Alexa Fluor 488- or 555-conjugated secondary antibodies (1:100, Thermo Fisher Scientific) and followed by staining with 1 μg/mL 4',6-Diamidino-2-phenylindole (DAPI) (Invitrogen, D3571). For chromosome spread staining, slides were incubated with primary antibodies anti-γH2AX (1:100, rabbit IgG, cell signaling technology, 9718S), anti-SYCP3 (1:50, mouse IgG, Santa Cruz, sc-74569), secondary antibodies, and DAPI as above. For detecting the acrosome, FITC-conjugated PNA (1:500, Vector laboratories, L7381) was used to stain sections followed by DAPI. For TUNEL staining, assays were performed using CoraLite®488 Plus TUNEL Assay Apoptosis Detection Kit (Proteintech, PF00006) following the manufacturer's instructions.

Embryoid bodies (EBs) at the indicated time were fixed with 4% PFA for 2 hours at 4 °C. After washing with PBST, EBs were permeabilized and blocked with 0.3% Triton X-100 solution and 10% normal donkey serum for 1 hour at RT. Then, primary antibodies anti-AP2γ (1:50, mouse IgG, Santa Cruz, sc-1262) and anti-Sox2 (1:100, rabbit IgG, Reprocell, 09-0024) were incubated with EBs at 4 °C overnight. After washing three times with PBST, EBs were incubated with secondary antibodies, followed by staining with DAPI.

All images were captured using a Zeiss LSM 710 confocal microscope (Carl Zeiss), and the fluorescence intensity was analyzed using Zeiss Zen 3.9 software.

RT-qPCR

Total RNAs from EpiLCs and PGCLCs were extracted using Trizol (Fisher Scientific, 15596018) and converted to cDNA using qScript (Quanta). Relative gene expression levels were analyzed with PowerUp™ SYBR™ Green Master Mix on the QuantStudio 5 PCR system (Life Technologies Inc.). Gene expression levels were normalized to *Gapdh*. The primers used are listed in Supplementary Table 1.

Western blot analysis

Cells were lysed in RIPA buffer (Boston BioProducts, Inc.) supplied with PMSF (Roche, 11359061001) and protease inhibitor cocktail (Sigma, P8340). Protein concentration was measured by Bradford assay (Thermo Fisher Scientific, 23246). The protein amounts were adjusted across samples, and then 4 × LDS sample buffer (GenScript, M00676-10) was added. Samples were boiled at 95 °C for 5 min. Proteins were separated on GenScript's SurePAGETM Bis-Tris gels and blotted on the Immobilon-P transfer membrane (Millipore). The membrane was blocked with 5% skim milk and incubated with primary antibodies: anti-Nanog (1:500, rabbit IgG, Bethyl/Fisher, A300-397A), anti-Gapdh (1:1000, rabbit IgG, ProteinTech, 10494-1-AP), anti-HA tag (1:1000, rabbit IgG, Abcam, ab9110), anti-β-actin (1:1000, mouse IgG, Sigma-

Aldrich, clone AC-15, A5441), anti-Otx2 (1:1000, rabbit IgG, Abcam, ab21990), anti-Prdm1 (1:1,000, mouse IgG, Sigma-Aldrich, clone 5E7, SAB5300402), anti-Tex10 (1:1000, rabbit IgG, Thermo Fisher, 720257), anti-Vinculin (1:10000, rabbit IgG, Abcam, ab129002), and anti-Psmd7 (1:1000, mouse IgG, Santa Cruz, sc-390705). After washing with TBST (TBS with 0.1% Tween-20), the blots were incubated with a secondary antibody and detected using Medical Film Processor (SRX-101A) or ImageQuant LAS 4000 (GE Healthcare).

Transfection and lentiviral infection

Transfection of cells was performed using lipofectamine 3000 according to the manufacturer's instructions. The production of lentivirus and viral infection was performed as described[88]. Psmd7 plasmid used for ectopic overexpression was purchased from NovoPro (Cat. 749214-1). TCF/Lef:H2B-GFP plasmid used to read out the Wnt signaling response was a kind gift from Dr. Anna-Katerina Hadjantonakis (Memorial Sloan Kettering Cancer Center).

Single-cell RNA sequencing and data analysis

Testes were isolated from 8-week-old male mice. EBs were treated without or with dTAG13 for two days (D2EBs and **d**D2EBs). Cell suspensions were treated as in FACS as above. Samples were filtered with a 40-µm (Falcon, 352340) cell strainer, and filtered cells were used for single-cell sequencing in the genomic core facility of Columbia University. Briefly, 10x Genomics Chromium Single Cell 3' Reagent Kits v3.1 Chemistry with Dual Indexing were used for library preparation according to the manufacturer's instructions, and the NovaSeq 6000 was used for sequencing (2x100bp).

Single-cell RNA-seq reads were aligned to the mm10 genome for generating expression matrix using Cell Ranger (V8.0.1), and the produced data were further filtered using Seurat (V5.0.1) to exclude cells with fewer than 200 genes expressed and >50% of total expression from mitochondrial genes. Through the above steps, 17,816 cells from control (*Tex10*$^{+/+}$*; Stra8-iCre*) and 11,408 cells from cKO (*Tex10*$^{fl/-}$*; Stra8-iCre*) mouse testes for spermatogenesis analysis. 17,958 cells from control (D2EBs) and 11,644 cells from KO (**d**D2EBs) EBs for PGCLC specification/survival analysis. To remove the batch effect, the top 2000 highly variable genes were used for canonical correlation analysis implemented in Seurat (V5.0.1).

Bulk RNA-seq and data analysis

The whole testis samples were isolated from control (*Tex10*$^{fl/fl}$) and Tex10-cKO (*Tex10*$^{fl/-}$*; Stra8-iCre*) 8-week-old male mice. The whole EBs treated without or with dTAG13 for two (D2EBs or **d**D2EBs) and four days (D4EBs or **d**D4EBs) were collected. Too few cells survived after dTAG13 treatment for six days, so they were not collected. Total RNA was extracted with Trizol, and then RNA-seq libraries were made with 100 ng RNA using the Ovation Mouse RNA-seq kit (NuGEN, #0348-32) according to the manufacturer's protocol. Tex10 overexpression and control mESCs were transfected with PiggyBac FLAG-Tex10 plasmid and empty vector (EV) plasmid, respectively[20]. The overexpression was first confirmed by western blotting analysis (Fig. S8a). Then, confirmed cells were used for in vitro PGC specification. Cells at EpiLC, D2, D4, and D6EBs were collected. Total RNA was extracted using Trizol and followed by library preparation using Universal Plus mRNA-Seq with NuQuant Kit (TECAN, 0520-A01) according to the manufacturer's protocol. For low-input bulk RNA-seq, the purified spermatogenic cells from 8-week-old testes and PGCLCs from day2 and day6 EBs (D2EBs vs. **d**D2EBs, D2EV vs. D2OE and D6EV vs. D6OE) were collected by **FASC** as above. Total RNA was extracted using Trizol and followed by library preparation using SMART-Seq® HT PLUS Kit (Takara, R400749) according to the manufacturer's protocol. Biological duplicates were prepared for all samples. Libraries were sequenced on the HiSeq 4000 to obtain paired-end 150 nucleotides read length.

RNA-seq reads were aligned to the mouse mm10 genome using Bowtie2 (v2.3.4.3), and aligned bam files were sorted by name using the parameter -n. Next, we used the HTSeq software (v0.11.2) and mm10 annotation file from GENCODE to count reads for each gene using parameters -r name -f bam, and BioMart[89] to retrieve corresponding genes names. Finally, read counts were normalized with the trimmed mean of M-values (TMM) method[90] using edgeR (v3.26.8)[91] or the fragments per kilobase per million mapped reads (FPKM) method using Cufflinks (v2.2.1) for differential expression analysis. Gene ontology analysis was performed using DAVID. Gene set enrichment analysis was performed using GSEA software (v4.3.3).

ChIP-qPCR, ChIP-seq, and data analysis

ChIP-qPCR and ChIP-seq samples were prepared following the instructions of SampleChIP^{R} Enzymatic Chromatin IP Kit (Cell Signaling, #9005). Briefly, 4×10^6 cells per ChIP were fixed in 1% PFA (RT, 10 min), quenched with 1 volume of 250 mM glycine (RT, 5 min), and rinsed with chilled PBS buffer twice before storage at −80 °C. After thawing the cells on ice, fixed cells were lysed to pellet nuclei, and 0.5 µL micrococcal nuclease per sample was used to digest DNA. Digestion was stopped by adding 10 µL 0.5 M EDTA per sample and placed on ice for 2 min. The nuclei pellet was then collected by 16,000 × *g* at 4 °C for 1 min. Pellets from individual samples were resuspended in 100 µL 1× ChIP buffer and incubated on ice for 10 min. Samples were sonicated five times (30-s pulses with 30-s break intervals) using the Bioruptor water bath sonicator (Diagenode). Chromatin extracts were centrifuged at 9400 × *g* for 10 min at 4 °C. The supernatant was transferred to a new tube for the following IP experiments. For each sample, 100 µL digested chromatin was diluted into 400 µL 1× ChIP buffer. We used two cell clones, C1 and C2, as biological replicates and 10 µL of diluted chromatin was used as 2% Input. For each IP, anti-HA tag antibody (6 µg per ChIP, Abcam, ab9110), H3K4me3 antibody (6 µg per ChIP, Abcam, ab8580), or normal rabbit IgG (6 µg per ChIP, Cell Signaling Tech., 2729 P) as a negative control was incubated with digested chromatin overnight with rotation at 4 °C and then incubated with 30 µL Protein G magnetic beads for 2 h at 4 °C with rotation. Using the magnetic separation rack, beads were washed with low-salt buffer three times and high-salt buffer one time at 4 °C with rotation. For input samples, 150 µL ChIP elution buffer was added and put aside at RT. For IP samples, 150 µL ChIP elution buffer was added and incubated at 65 °C for 30 min with gentle vortexing. A magnetic separation rack was used to collect the solution. Reverse crosslinking was done at 65 °C for 6 h by adding 2 µL Proteinase K and 6 µL 5 M NaCl. Finally, DNA was purified for qPCR analysis or library preparation using NEBNext® Ultra™ II DNA Library Prep (E7103S). Once prepared, the library was sequenced using HiSeq 4000 with paired-end 150 nucleotides read length.

ChIP-seq reads were mapped to the mm10 genome using Bowtie2 (v2.3.4.3), and PCR duplicates were removed using Samtools (v1.9). Peaks were then called using MACS2 (v2.1.2) to compare IP samples with input samples; only peaks called from both replicates were kept. Finally, annotation was done using the script annotatePeaks.pl of HOMER[92].

Gene pattern analysis on naive-to-primed pluripotency transition data

Naive-to-primed pluripotency transition data were downloaded from GSE117896[93] and normalized with the TMM method using edgeR. Genes with a TMM value equal to 0 were removed. To obtain up-down regulation pattern genes, parameters, $\log_2$FC(H36/H12) > 0.2, $\log_2$FC(H72/H36) < −0.2, and FDR(H72/H36) < 0.05 were used to select genes. H36/H12 and H72/H36 represent the fold changes of gene expression at 36 h vs. at 12 h and gene expression at 72 h vs. at 36 h, respectively. We systematically analyzed the 0 to 72 h time-course RNA-seq data[93] of naive-to-primed pluripotency transition and filtered genes with the up-down regulation pattern within the critical PGCLC specification time window using our own RNA-seq data (Supplementary Data 6) to exclude

genes that were significantly decreased at Day 2 PGCLC vs. EpiLC stage. We identified 187 genes (Supplementary Data 16) with the up-down regulation pattern containing potential PGCLC specifiers. For these 187 genes, we further conducted gene prioritization analysis based on their expression in 30 tissues/cells (see the below section).

Gene prioritization analysis

For the above 187 genes, gene expression values of 159 genes could be curated from the published literature[94], of which the PGC dataset was curated from GSE60377[95]. The PGCs were isolated from E13.5 gonads and sorted with the germ cell surface marker SSEA1[96]. The analysis was done on above 159 genes (Fig. S1g) as follows: 1) For each gene, 30 curated tissues/cells, mainly including early embryos (such as 4-cell, 8-cell, morula, and blastocyst), ESCs, epiblast, and PGCs (male/female), were ranked based on the gene expression from high to low; 2) If the male/female PGCs were ranked the top five, its corresponding genes from step 1 were collected and used for further analysis; 3) Within genes collected by step 2, those with male/female PGCs ranked the first were chosen as candidates.

The gene set activity analysis

Pluripotency, PGC regulator, mesoderm, endoderm, and ectoderm gene sets were curated in the literature[8,20] and R&D database (Supplementary Data 17). First, for each gene in a specific category, such as pluripotency, the $\log_2$FC of the gene was calculated. Then, the mean $\log_2$FC of all genes in a category was regarded as the overall activity value.

Statistics and reproducibility

Statistical analysis was performed using R (version 4.3.2) or Prism (version 9.5.0). Data are presented as mean ± SD. A two-tailed student's *t*-test or one-way ANOVA was used to determine the statistical significance. **** for p-value < 0.0001, *** for p-value < 0.001, ** for p-value < 0.01, * for p-value < 0.05, and ns for p-value > 0.05. For all the histology, immunofluorescence, and western blot experiments, at least three independent repetitions were performed with consistent results, and representative data were presented. Source data are provided as a Source Data file.

Inclusion and diversity

We worked to ensure diversity in experimental samples through the selection of multiple cell lines and clones.

Reporting summary

Further information on research design is available in the Nature Portfolio Reporting Summary linked to this article.

Data availability

All high-throughput ChIP-seq and RNA-seq data generated in this study are available at the Gene Expression Omnibus under accession code GSE180801, GSE190072, and GSE288186 [https://www.ncbi.nlm.nih.gov/geo/query/acc.cgi?acc=GSE288186]. The previously published accession codes used in this study are GSE117473, DDBJ: DRA006497, GSE148032, GSE75738, GSE145467, GSE6872, and GSE30056. Source data are provided with this paper.

References

1. Eisenberg, M. L. et al. Male infertility. *Nat. Rev. Dis. Prim.* **9**, 49 (2023).
2. Mousavi, S. A., Masoumi, S. Z., Keramat, A., Pooralajal, J. & Shobeiri, F. Assessment of questionnaires measuring quality of life in infertile couples: a systematic review. *J. Reprod. Infertil.* **14**, 110–119 (2013).
3. Robinson, M., Sparanese, S., Witherspoon, L. & Flannigan, R. Human in vitro spermatogenesis as a regenerative therapy - where do we stand? *Nat. Rev. Urol.* **20**, 461–479 (2023).
4. Chao, H. H., Zhang, Y., Dong, P. Y., Gurunathan, S. & Zhang, X. F. Comprehensive review on the positive and negative effects of various important regulators on male spermatogenesis and fertility. *Front. Nutr.* **9**, 1063510 (2022).
5. Dabaja, A. A. & Schlegel, P. N. Medical treatment of male infertility. *Transl. Androl. Urol.* **3**, 9–16 (2014).
6. Chen, D., Gell, J. J., Tao, Y., Sosa, E. & Clark, A. T. Modeling human infertility with pluripotent stem cells. *Stem Cell Res.* **21**, 187–192 (2017).
7. Murakami, K. et al. NANOG alone induces germ cells in primed epiblast in vitro by activation of enhancers. *Nature* **529**, 403–407 (2016).
8. Hackett, J. A. et al. Tracing the transitions from pluripotency to germ cell fate with CRISPR screening. *Nat. Commun.* **9**, 4292 (2018).
9. Tang, W. W., Kobayashi, T., Irie, N., Dietmann, S. & Surani, M. A. Specification and epigenetic programming of the human germ line. *Nat. Rev. Genet.* **17**, 585–600 (2016).
10. Magnusdottir, E. et al. A tripartite transcription factor network regulates primordial germ cell specification in mice. *Nat. Cell Biol.* **15**, 905–915 (2013).
11. Golestaneh, N. et al. Wnt signaling promotes proliferation and stemness regulation of spermatogonial stem/progenitor cells. *Reproduction* **138**, 151–162 (2009).
12. Takase, H. M. & Nusse, R. Paracrine Wnt/beta-catenin signaling mediates proliferation of undifferentiated spermatogonia in the adult mouse testis. *Proc. Natl Acad. Sci. USA* **113**, E1489–E1497 (2016).
13. Kumar, M., Atkins, J., Cairns, M., Ali, A. & Tanwar, P. S. Germ cell-specific sustained activation of Wnt signalling perturbs spermatogenesis in aged mice, possibly through non-coding RNAs. *Oncotarget* **7**, 85709–85727 (2016).
14. Chassot, A. A. et al. Constitutive WNT/CTNNB1 activation triggers spermatogonial stem cell proliferation and germ cell depletion. *Dev. Biol.* **426**, 17–27 (2017).
15. Kehler, J. et al. Oct4 is required for primordial germ cell survival. *EMBO Rep.* **5**, 1078–1083 (2004).
16. Campolo, F. et al. Essential role of Sox2 for the establishment and maintenance of the germ cell line. *Stem Cells* **31**, 1408–1421 (2013).
17. Buecker, C. et al. Reorganization of enhancer patterns in transition from naive to primed pluripotency. *Cell Stem Cell* **14**, 838–853 (2014).
18. Acampora, D., Di Giovannantonio, L. G. & Simeone, A. Otx2 is an intrinsic determinant of the embryonic stem cell state and is required for transition to a stable epiblast stem cell condition. *Development* **140**, 43–55 (2013).
19. Zhang, J. et al. OTX2 restricts entry to the mouse germline. *Nature* **562**, 595–599 (2018).
20. Ding, J. et al. Tex10 coordinates epigenetic control of super-enhancer activity in pluripotency and reprogramming. *Cell Stem Cell* **16**, 653–668 (2015).
21. Rehm, H. L. et al. ClinGen-the clinical genome resource. *N. Engl. J. Med.* **372**, 2235–2242 (2015).
22. Sieper, M. H. et al. Scrutinizing the human TEX genes in the context of human male infertility. *Andrology* **12**, 570–584 (2024).
23. Zhao, J. et al. Cell-fate transition and determination analysis of mouse male germ cells throughout development. *Nat. Commun.* **12**, 6839 (2021).
24. Ma, B. et al. Molecular characteristics of early-stage female germ cells revealed by RNA sequencing of low-input cells and analysis of genome-wide DNA methylation. *DNA Res.* **26**, 105–117 (2019).
25. Hayashi, K., Ohta, H., Kurimoto, K., Aramaki, S. & Saitou, M. Reconstitution of the mouse germ cell specification pathway in culture by pluripotent stem cells. *Cell* **146**, 519–532 (2011).
26. Sadate-Ngatchou, P. I., Payne, C. J., Dearth, A. T. & Braun, R. E. Cre recombinase activity specific to postnatal, premeiotic male germ cells in transgenic mice. *Genesis* **46**, 738–742 (2008).
27. Paniagua, R., Nistal, M., Amat, P., Rodriguez, M. C. & Martin, A. Seminiferous tubule involution in elderly men. *Biol. Reprod.* **36**, 939–947 (1987).

28. Fang, X. et al. Proteomics and single-cell RNA analysis of Akap4-knockout mice model confirm indispensable role of Akap4 in spermatogenesis. *Dev. Biol.* **454**, 118–127 (2019).
29. Kashiwabara, S. et al. Regulation of spermatogenesis by testis-specific, cytoplasmic poly(A) polymerase TPAP. *Science* **298**, 1999–2002 (2002).
30. Zhuang, T., Kashiwabara, S., Noguchi, J. & Baba, T. Transgenic expression of testis-specific poly(A) polymerase TPAP in wild-type and TPAP-deficient mice. *J. Reprod. Dev.* **50**, 207–213 (2004).
31. Liu, D. et al. Cyclin A1 is required for meiosis in the male mouse. *Nat. Genet.* **20**, 377–380 (1998).
32. Liu, D., Liao, C. & Wolgemuth, D. J. A role for cyclin A1 in the activation of MPF and G2-M transition during meiosis of male germ cells in mice. *Dev. Biol.* **224**, 388–400 (2000).
33. Salazar, G. et al. Induction of apoptosis involving multiple pathways is a primary response to cyclin A1-deficiency in male meiosis. *Dev. Dyn.* **234**, 114–123 (2005).
34. Zheng, M. et al. TULP2, a new RNA-binding protein, is required for mouse spermatid differentiation and male fertility. *Front. cell Dev. Biol.* **9**, 623738 (2021).
35. Tokuhiro, K. et al. OAZ-t/OAZ3 is essential for rigid connection of sperm tails to heads in mouse. *PLoS Genet.* **5**, e1000712 (2009).
36. Yuan, S. et al. Spata6 is required for normal assembly of the sperm connecting piece and tight head-tail conjunction. *Proc. Natl Acad. Sci. USA* **112**, E430–E439 (2015).
37. Yang, K. et al. The small heat shock protein ODF1/HSPB10 is essential for tight linkage of sperm head to tail and male fertility in mice. *Mol. Cell Biol.* **32**, 216–225 (2012).
38. Woolley, D. M. Flagellar oscillation: a commentary on proposed mechanisms. *Biol. Rev. Camb. Philos. Soc.* **85**, 453–470 (2010).
39. Fawcett, D. W. & Phillips, D. M. The fine structure and development of the neck region of the mammalian spermatozoon. *Anat. Rec.* **165**, 153–164 (1969).
40. Chen, S. R. et al. The control of male fertility by spermatid-specific factors: searching for contraceptive targets from spermatozoon's head to tail. *Cell Death Dis.* **7**, e2472 (2016).
41. Shirley, C. R., Hayashi, S., Mounsey, S., Yanagimachi, R. & Meistrich, M. L. Abnormalities and reduced reproductive potential of sperm from Tnp1- and Tnp2-null double mutant mice. *Biol. Reprod.* **71**, 1220–1229 (2004).
42. Martianov, I. et al. Distinct functions of TBP and TLF/TRF2 during spermatogenesis: requirement of TLF for heterochromatic chromocenter formation in haploid round spermatids. *Development* **129**, 945–955 (2002).
43. De Vries, W. N. et al. Expression of Cre recombinase in mouse oocytes: a means to study maternal effect genes. *Genesis* **26**, 110–112 (2000).
44. Hodzic, A. et al. Transcriptomic signatures for human male infertility. *Front. Mol. Biosci.* **10**, 1226829 (2023).
45. Platts, A. E. et al. Success and failure in human spermatogenesis as revealed by teratozoospermic RNAs. *Hum. Mol. Genet.* **16**, 763–773 (2007).
46. Zhao, L. et al. Single-cell analysis of developing and azoospermia human testicles reveals central role of Sertoli cells. *Nat. Commun.* **11**, 5683 (2020).
47. Di Persio, S. et al. Single-cell RNA-seq unravels alterations of the human spermatogonial stem cell compartment in patients with impaired spermatogenesis. *Cell Rep. Med.* **2**, 100395 (2021).
48. Gaysinskaya, V., Soh, I. Y., van der Heijden, G. W. & Bortvin, A. Optimized flow cytometry isolation of murine spermatocytes. *Cytom. Part J. Int. Soc. Anal. Cytol.* **85**, 556–565 (2014).
49. Miller, M. P., Unal, E., Brar, G. A. & Amon, A. Meiosis I chromosome segregation is established through regulation of microtubule-kinetochore interactions. *Elife* **1**, e00117 (2012).
50. Lehti, M. S. & Sironen, A. Formation and function of the manchette and flagellum during spermatogenesis. *Reproduction* **151**, R43–R54 (2016).
51. Ohinata, Y. et al. Blimp1 is a critical determinant of the germ cell lineage in mice. *Nature* **436**, 207–213 (2005).
52. Nabet, B. et al. The dTAG system for immediate and target-specific protein degradation. *Nat. Chem. Biol.* **14**, 431–441 (2018).
53. Morgani, S. M. & Hadjantonakis, A. K. Quantitative analysis of signaling responses during mouse primordial germ cell specification. *Biol. Open* **10**, bio058741 (2021).
54. Clevers, H. & Nusse, R. Wnt/beta-catenin signaling and disease. *Cell* **149**, 1192–1205 (2012).
55. Tezuka, N., Brown, A. M. & Yanagawa, S. GRB10 binds to LRP6, the Wnt co-receptor and inhibits canonical Wnt signaling pathway. *Biochem. Biophys. Res. Commun.* **356**, 648–654 (2007).
56. Rattner, A. et al. A family of secreted proteins contains homology to the cysteine-rich ligand-binding domain of frizzled receptors. *Proc. Natl. Acad. Sci. USA* **94**, 2859–2863 (1997).
57. Fararjeh, A. S. et al. Proteasome 26S subunit, non-ATPase 3 (PSMD3) regulates breast cancer by stabilizing HER2 from degradation. *Cancers* **11**, 527 (2019).
58. Aberle, H., Bauer, A., Stappert, J., Kispert, A. & Kemler, R. beta-catenin is a target for the ubiquitin-proteasome pathway. *EMBO J.* **16**, 3797–3804 (1997).
59. Kominami, K. et al. Yeast counterparts of subunits S5a and p58 (S3) of the human 26S proteasome are encoded by two multicopy suppressors of nin1-1. *Mol. Biol. Cell* **8**, 171–187 (1997).
60. Yi, J. J. et al. The autism-linked UBE3A T485A mutant E3 ubiquitin ligase activates the Wnt/beta-catenin pathway by inhibiting the proteasome. *J. Biol. Chem.* **292**, 12503–12515 (2017).
61. Steinhart, Z. & Angers, S. Wnt signaling in development and tissue homeostasis. *Development* **145**, dev146589 (2018).
62. Kimura, T. et al. Induction of primordial germ cell-like cells from mouse embryonic stem cells by ERK signal inhibition. *Stem Cells* **32**, 2668–2678 (2014).
63. Mochizuki, K. et al. Repression of somatic genes by selective recruitment of HDAC3 by BLIMP1 is essential for mouse primordial germ cell fate determination. *Cell Rep.* **24**, 2682–2693.e2686 (2018).
64. Rivas, B., Huang, Z. & Agoulnik, A. I. Normal fertility in male mice with deletion of beta-catenin gene in germ cells. *Genesis* **52**, 328–332 (2014).
65. Chang, Y. F., Lee-Chang, J. S., Harris, K. Y., Sinha-Hikim, A. P. & Rao, M. K. Role of beta-catenin in post-meiotic male germ cell differentiation. *PloS One* **6**, e28039 (2011).
66. Subramanian, A. et al. Gene set enrichment analysis: a knowledge-based approach for interpreting genome-wide expression profiles. *Proc. Natl Acad. Sci. USA* **102**, 15545–15550 (2005).
67. Liberzon, A. et al. The Molecular Signatures Database (MSigDB) hallmark gene set collection. *Cell Syst.* **1**, 417–425 (2015).
68. Tokue, M. et al. SHISA6 confers resistance to differentiation-promoting Wnt/beta-catenin signaling in mouse spermatogenic stem cells. *Stem Cell Rep.* **8**, 561–575 (2017).
69. Chen, S. R. et al. Does murine spermatogenesis require WNT signalling? A lesson from Gpr177 conditional knockout mouse models. *Cell Death Dis.* **7**, e2281 (2016).
70. Arnold, S. J. et al. Brachyury is a target gene of the Wnt/beta-catenin signaling pathway. *Mech. Dev.* **91**, 249–258 (2000).
71. Aramaki, S. et al. A mesodermal factor, T, specifies mouse germ cell fate by directly activating germline determinants. *Dev. Cell* **27**, 516–529 (2013).
72. Boyer, L. A. et al. Core transcriptional regulatory circuitry in human embryonic stem cells. *Cell* **122**, 947–956 (2005).
73. Festuccia, N., Osorno, R., Wilson, V. & Chambers, I. The role of pluripotency gene regulatory network components in mediating

transitions between pluripotent cell states. *Curr. Opin. Genet. Dev.* **23**, 504–511 (2013).
74. Yamaguchi, S. et al. Conditional knockdown of Nanog induces apoptotic cell death in mouse migrating primordial germ cells. *Development* **136**, 4011–4020 (2009).
75. Mitsunaga, K. et al. Loss of PGC-specific expression of the orphan nuclear receptor ERR-beta results in reduction of germ cell number in mouse embryos. *Mech. Dev.* **121**, 237–246 (2004).
76. Mitsui, K. et al. The homeoprotein Nanog is required for maintenance of pluripotency in mouse epiblast and ES cells. *Cell* **113**, 631–642 (2003).
77. Nichols, J. et al. Formation of pluripotent stem cells in the mammalian embryo depends on the POU transcription factor Oct4. *Cell* **95**, 379–391 (1998).
78. Avilion, A. A. et al. Multipotent cell lineages in early mouse development depend on SOX2 function. *Genes Dev.* **17**, 126–140 (2003).
79. Mikedis, M. M. & Downs, K. M. PRDM1/BLIMP1 is widely distributed to the nascent fetal-placental interface in the mouse gastrula. *Dev. Dyn.* **246**, 50–71 (2017).
80. Von Meyenn, F. & Reik, W. Forget the parents: epigenetic reprogramming in human germ cells. *Cell* **161**, 1248–1251 (2015).
81. Donovan M. F., Bordoni B. Embryology, yolk sac. In: *StatPearls* (2021).
82. Nowotschin, S. et al. The emergent landscape of the mouse gut endoderm at single-cell resolution. *Nature* **569**, 361–367 (2019).
83. Zhang, Y. et al. Dynamic epigenomic landscapes during early lineage specification in mouse embryos. *Nat. Genet.* **50**, 96–105 (2018).
84. Hill, P. W. S. et al. Epigenetic reprogramming enables the transition from primordial germ cell to gonocyte. *Nature* **555**, 392–396 (2018).
85. Kurimoto, K. et al. Complex genome-wide transcription dynamics orchestrated by Blimp1 for the specification of the germ cell lineage in mice. *Genes Dev.* **22**, 1617–1635 (2008).
86. Murase, Y. et al. In vitro reconstitution of epigenetic reprogramming in the human germ line. *Nature* **631**, 170–178 (2024).
87. Treter, J. et al. Washing-resistant surfactant coated surface is able to inhibit pathogenic bacteria adhesion. *Appl. Surf. Sci.* **303**, 147–154 (2014).
88. Ivanova, N. et al. Dissecting self-renewal in stem cells with RNA interference. *Nature* **442**, 533–538 (2006).
89. Durinck, S. et al. BioMart and Bioconductor: a powerful link between biological databases and microarray data analysis. *Bioinformatics* **21**, 3439–3440 (2005).
90. Robinson, M. D. & Oshlack, A. A scaling normalization method for differential expression analysis of RNA-seq data. *Genome Biol.* **11**, R25 (2010).
91. Robinson, M. D., McCarthy, D. J. & Smyth, G. K. edgeR: a Bioconductor package for differential expression analysis of digital gene expression data. *Bioinformatics* **26**, 139–140 (2010).
92. Heinz, S. et al. Simple combinations of lineage-determining transcription factors prime cis-regulatory elements required for macrophage and B cell identities. *Mol. Cell* **38**, 576–589 (2010).
93. Yang, P. et al. Multi-omic profiling reveals dynamics of the phased progression of pluripotency. *Cell Syst.* **8**, 427–445.e410 (2019).
94. Hutchins, A. P. et al. Models of global gene expression define major domains of cell type and tissue identity. *Nucleic Acids Res.* **45**, 2354–2367 (2017).
95. Liu, S. et al. Setdb1 is required for germline development and silencing of H3K9me3-marked endogenous retroviruses in primordial germ cells. *Genes Dev.* **28**, 2041–2055 (2014).
96. Durcova-Hills, G. et al. Immunomagnetic isolation of primordial germ cells and the establishment of embryonic germ cell lines in the mouse. *Cloning* **1**, 217–224 (1999).
97. Ferrer-Vaquer, A. et al. A sensitive and bright single-cell resolution live imaging reporter of Wnt/ss-catenin signaling in the mouse. *BMC Dev. Biol.* **10**, 121 (2010).

Acknowledgements

We thank Dr. Kat Hadjantonakis for the TCF/Lef:H2B-GFP reporter construct. The research is supported by a shared instrumentation grant for the Influx (S10OD020056) and LSRII (S10RR027050) Flow Cytometer to the Columbia Center for Translational Immunology Flow Cytometry Core. This research also used the Genomics and High Throughput Screening Shared Resource funded partly through the NIH/NCI Cancer Center Support Grant P30CA013696 and Grant Number UL1TR001873 by the National Center for Advancing Translational Sciences, NIH. Research in the Wang laboratory is supported by NIH (HD095938, HD097268, and HD114122) and NYSTEM (C32583GG and C32569GG).

Author contributions

F.Y., J.Y., and F.M. designed the experiments. F.Y., J.Y., F.M., Z.H., R.Z., D.L., and X.S. performed the experiments. J.Y., V.M., and X.H. performed the computational analysis. F.Y. and J.Y. wrote the manuscript. H.Z. provided reagents and experimental support. J.W. conceived, designed, supervised the studies, and wrote and approved the final manuscript.

Competing interests

The authors declare no competing interests. None of the contents of this manuscript has been previously published or are under consideration elsewhere. All the authors have read and approved the final version of the manuscript before submission.

Additional information

Supplementary information The online version contains supplementary material available at https://doi.org/10.1038/s41467-025-57165-2.

Correspondence and requests for materials should be addressed to Jianlong Wang.

Peer review information *Nature Communications* thanks the anonymous reviewers for their contribution to the peer review of this work. A peer review file is available.